www.nautilos-h2020.eu

Organisation NIVA
Department Oceanography

D6.2

Report on results and methodology of calibration / validation experiments performed in T6.2

Date: 26/11/2023
Doc. Version: 1.1
doi : 10.5281/zenodo.10669815

This project has received funding from the European Union's Horizon 2020 research and innovation programme under grant agreement No. 101000825 (NAUTILOS). This output reflects only the author's view and the European Union cannot be held responsible for any use that may be made of the information contained therein.

Document Control Information

Settings	Value
Deliverable Title	Report on results and methodology of calibration / validation experiments performed in T6.2
Work Package Title	Calibration, Validation and Scenario Testing
Deliverable number	D6.2
Description	Laboratory calibration and validation of instruments developed in WP4
Lead Beneficiary	NIVA
Lead Authors	Sabine Marty, Andrew King, Manolis Ntoumas
Contributors	Damien Malardé, Christos Tsabaris, Jana Fahning, Elena Martinez, Bert Van Bavel, Peter Cristofolini, Kai Sørensen, Nicholas Roden, Carole Barus
Submitted by	Sabine Marty
Doc. Version (Revision number)	1.1
Sensitivity (Security):	Public
Date:	26.11.2023
doi:	10.5281/zenodo.10669815

Document Approver(s) and Reviewer(s):

NOTE: All Approvers are required. Records of each approver must be maintained. All Reviewers in the list are considered required unless explicitly listed as Optional.

Name	Role	Action	Date
Ivan Alonso	Review team#2	*Approve*	21.11.2023

Document history:

The Document Author is authorized to make the following types of changes to the document without requiring that the document be re-approved:

- Editorial, formatting, and spelling
- Clarification

To request a change to this document, contact the Document Author or Owner.

Changes to this document are summarized in the following table in reverse chronological order (latest version first).

Revision	Date	Created by	Short Description of Changes
V1.1	26.11.2023	Andrew King	Final version with updates
V1.0	15.11.2023	Sabine Marty	Draft
V0.1	26.05.2023	Sabine Marty	Change in the structure of the document.
V0	01.05.2023	Sabine Marty	Skeleton created

Configuration Management: Document Location

The latest version of this controlled document is stored in <location>.

Nature of the deliverable		
R	Report	X
DEC	Websites, patents, filing, etc.	
DEM	Demonstrator	
O	Other	

Dissemination level		
PU	Public	X
CO	Confidential, only for members of the consortium (including the Commission Services)	

ACKNOWLEDGEMENT

This report forms part of the deliverables from the NAUTILOS project which has received funding from the European Union's Horizon 2020 research and innovation programme under grant agreement No 101000825. The Community is not responsible for any use that might be made of the content of this publication.

NAUTILOS - New Approach to Underwater Technologies for Innovative, Low-cost Ocean observation is an H2020 project funded under the Future of Seas and Oceans Flagship Initiative, coordinated by the National Research Council of Italy (CNR, Consiglio Nazionale delle Ricerche). It brings together a group of 21 entities from 11 European countries with multidisciplinary expertise ranging from ocean instrumentation development and integration, ocean sensing and sampling instrumentation, data processing, modelling and control, operational oceanography and biology and ecosystems and biogeochemistry such, water and climate change science, technological marine applications and research infrastructures.

NAUTILOS will fill-in marine observation and modelling gaps for chemical, biological and deep ocean physics variables through the development of a new generation of cost-effective sensors and samplers, the integration of the aforementioned technologies within observing platforms and their deployment in large-scale demonstrations in European seas. The fundamental aim of the project will be to complement and expand current European observation tools and services, to obtain a collection of data at a much higher spatial resolution, temporal regularity and length than currently available at the European scale, and to further enable and democratise the monitoring of the marine environment to both traditional and non-traditional data users.

NAUTILOS is one of two projects included in the EU´s efforts to support the European Strategy for Plastics in a Circular Economy by supporting the demonstration of new and innovative technologies to measure the Essential Ocean Variables (EOV).

More information on the project can be found at: http://www.nautilos-h2020.eu.

COPYRIGHT

TABLE OF CONTENTS

ACKNOWLEDGEMENT **4**

COPYRIGHT **4**

TABLE OF CONTENTS **5**

EXECUTIVE SUMMARY **7**

LIST OF FIGURES **7**

LIST OF TABLES **8**

LIST OF ACRONYMS AND ABBREVIATIONS **9**

I. INTRODUCTION TO SENSOR/PLATFORM TECHNOLOGY **10**

II. OBJECTIVES **10**

III. LABORATORY TESTS **10**

1. Carbonate system / ocean acidification sensors 10
   - 1.1. Objectives 11
   - 1.2. Calibration and validation references 11
   - 1.3. Description of the tests 13
   - 1.4. Results 13
2. Silicate sensor 17
   - 2.1. Objectives 18
   - 2.2. Calibration and validation references 18
   - 2.3. Description of the tests 19
   - 2.4. Results 20
3. Deep ocean CTD 21
   - 3.1. Objectives 22
   - 3.2. Calibration and validation references 23
   - 3.3. Description of the tests 25
   - 3.4. Results 29
4. Submersible Nano- and MicroPlastics Sampler (SuNaMiPS) 32
   - 4.1. Objectives 33
   - 4.2. Calibration and validation references 33
   - 4.3. Description of the tests 33
   - 4.4. Results 35
5. Low cost Microplastic sensor (LAMPO) 36
   - 5.1. Objectives 37
   - 5.2. Calibration and validation references 37
   - 5.3. Description of the tests 37

5.4. Results 40
6. Deep-ocean low-level radioactivity sensor 41
6.1. Objectives 41
6.2. Calibration and validation references 42
6.3. Description of the tests 42
6.4. Results 43
IV. SUMMARY 45
V. APPENDIX 1: REFERENCES AND RELATED DOCUMENTS 46

EXECUTIVE SUMMARY

This deliverable reports on WP6 calibration and validation tests for six cost-effective instruments developed in WP4 that measure variables related to physical, chemical, and microplastics Essential Ocean Variables (EOVs) and Marine Strategy Framework Directives (MSFDs). Each instrument - different sensor and sampling technologies - was tested under realistic experimental conditions to document performance in terms of how well sensors measured variables of interest and how well samplers collected targets of interest. This was an important step to ensure that instruments performed according to the needs and requirements of demonstration activities in WP7, both in terms of withstanding operations with seawater or submerged in seawater, and also that variables of interest were sufficiently measured and sampled.

LIST OF FIGURES

Figure 1: NAUTILOS Honeywell ISFET sensor with pressure housing. 11
Figure 2: Calibration coefficients for the CO2-HR sensor. Gas standards were pumped through the end cap enclosing the membrane until equilibration across the membrane had occurred. 12
Figure 3: pH values during ~24-hour in-tank test. Top panel shows temperature values from inside each sensor and reference temperature at in situ conditions (SBE38). Bottom panel shows pH values at in situ temperature, red dashed lines indicate timing of acid addition. 13
Figure 4: Response time of pH sensors after first acid addition. Dashed lines indicate how long measurements from each sensor take to reach 90% of the final value (t90). 14
Figure 5: pCO_2 values during ~24-hour in-tank test. Top panel shows temperature values from inside each sensor and reference temperature at in situ conditions (SBE38). Bottom panel shows pCO_2 values at in situ temperature, red dashed lines indicate timing of acid addition. 15
Figure 6: Response time of pCO_2 sensors after first acid addition. Dashed lines indicate how long measurements from each sensor take to reach 90% of the final value (t90). 16
Figure 7: Optimised design of Silicate in situ electrochemical sensor. 17
Figure 8: Silicate sensor equipped with funnel for laboratory experiments immersed in artificial seawater tank. 19
Figure 9: Calibration plots of silicate standards obtained with the electrochemical sensor. 20
Figure 10: Calibration plot of silicate sensor compared with results obtained with CRM. 21
Figure 11: NAUTILOS Deep Ocean CTD instrument. 23
Figure 12: The Poseidon calibration laboratory. The black calibration tanks to the left side of the picture. 24
Figure 13: Rate of temperature increase inside the PCL calibration tank. At times when the temperature appears to remain constant, the heater has been turned off in order to proceed to sampling for calibration. The red and blue lines denote fits to the heating rate performed at about 14:00-14:45 and 17:00-17:20, respectively. The maximum heating rates are estimated to about 4.3±0.2 °C hr^{-1}. 24
Figure 14: A snapshot of the software developed to facilitate the programming of the CT sensors, the upload and analysis of the data collected and to provide real-time monitoring of the calibration procedure. 26
Figure 15: The NAUTILOS CTD and other RBR CT sensors placed inside the PCL calibration tank. 26
Figure 16: The temperature calibration timeseries is presented in the upper panel. The panel below corresponds to the calibration window highlighted by the green oval. 27
Figure 17: The conductivity calibration timeseries is presented in the upper panel. The panel below corresponds to the calibration window highlighted by the green oval. 28
Figure 18: The NAUTILOS CTD placed horizontally inside the tank during the conductivity calibration experiment. 29
Figure 19: Calibration linear fit for CTD temperature sensor. 29
Figure 20: The temperature residuals before and after the calibration of the sensor. 30

Figure 21: Uncompensated long term measurement of conductivity (blue) at variable room temperature environment (red) and efficient temperature compensation of conductivity by experimentally determined TCC=2% /°C (black). 31
Figure 22: The conductivity residuals before the data process. 31
Figure 23: Calibration linear fit for CTD conductivity sensor. 32
Figure 24: The conductivity residuals before and after the calibration of the sensor. 32
Figure 25:The SuNaMiPS with external batteries attached - ready for deployment. 33
Figure 26: Sampler under testing conditions. 34
Figure 27: Difference of measured flow rate. 35
Figure 28: Difference in calculated volume. 35
Figure 29: Low cost microplastic sensor. 37
Figure 30: Microplastic sampler normal run mode. 38
Figure 31: Cross section of the microplastic detector with the fluidic pathway (left) and the green and red fluorescence detection channels on the photodiodes. 39
Figure 32: Characterization datasets recorded with the microplastic detector, for Nile red stained PET microplastic 100-150um (top) and yellow reference plastic spheres 40-45 um (bottom). 39
Figure 33: Deep-ocean low-level radioactivity sensor. 41
Figure 34: The pressure tests were performed in the “Demokritos” laboratory. 42
Figure 35: The energy calibrated spectrum using the Co-60 point standard source on log scale. 43
Figure 36: The energy calibrated spectrum using the Co-60 point standard source on linear scale. 43
Figure 37: The energy spectrum was acquired in the calibration tank. The detected radionuclides are indicated in the graph. Natural Radioactivity (thoron and radon progenies, K-40) and Artificial Radioactivity (Cs-137) is depicted (Cs-137 at 662 keV, Bi-214 at 609 and 1761 keV, Tl-208 at 583 and 2614 keV, K-40 at 1461 keV). 44

LIST OF TABLES

Table 1: pH values at in situ temperature. Both Durafet and Endress electrodes were calibrated to the first bottle sample. Mean absolute error (MAE), relative to bottle samples, is calculated for each ISFET sensor. 14
Table 2: pCO_2 (µatm) values at in situ temperature. Mean absolute error (MAE), relative to bottle samples, is calculated for each sensor. 16
Table 3: The concentrations of the standard solutions analysed with the silicate sensor and their standard deviations (SD). 18
Table 4: CRM composition (only silicate concentrations are indicated but samples contain phosphate, nitrate and nitrite as well). 18
Table 5: CRM analysis with silicate sensor and accuracy evaluation. 21
Table 6: ICTD WOCE Specifications source: salinometry.com 22
Table 7: Specifications of the NAUTILOS CTD instrument. 23
Table 8: Details of the reference instrumentation are shown. 25
Table 9: The components of the uncertainty budget of the temperature calibration are shown. 25
Table 10: Reference microplastic particles used for testing. 34
Table 11: Results of the water flow measurements. 36

List of Acronyms and Abbreviations

Abbreviation	Definition
CO_2	Carbon dioxide
CRM	Certified reference material
CSV	Comma separated value
CTD	Conductivity, temperature, depth
DIC	Dissolved inorganic carbon
DIC	Dissolved inorganic carbon
GeoMAREA	Gamma-ray spectrometer for in-situ MARine Environmental Applications
GOA-ON	Global Ocean Acidification Observing Network
GUM	Guide to the expression of Uncertainty in Measurement
HCl	Hydrochloric acid
ISFET	Ion Sensitive Field Effect Transistor
ITS-90	International temperature scale of 1990
JSON	JavaScript Object Notation
LAMPO	Low cost Microplastics sensor
MAE	Mean absolute error
MEMS	Micro Electronic Mechanical Systems
MERL	Marine Environmental Radioactivity Laboratory
NaOH	Sodium hydroxide
PA	Polyamide
PCB	Printed circuit board
PCL	POSEIDON Calibration Lab
pCO_2	Partial pressure of carbon dioxide
PE	Polyethylene
PET	Polyethylene terephthalate
PLC	Programmable logic controller
PP	Polypropylene
PS	Polystyrene
PVC	Polyvinyl chloride
RS-232	Recommended Standard 232
SMA	Simple moving average
SS	Stainless steel
SuNaMiPS	Submersible Nano- and MicroPlastics Sampler
TA	Total alkalinity
TCC	Temperature Coefficient of Conductivity
VINDTA	Versatile INstrument for the Determination of Total inorganic carbon and titration Alkalinity

I. INTRODUCTION TO SENSOR/PLATFORM TECHNOLOGY

This deliverable reports on calibration and validation of instruments developed in WP4 which were focused on physical, chemical, and microplastics variables. The instruments include carbonate chemistry/ocean acidification sensors (subtask 6.2.1), a silicate electrochemical sensor (subtask 6.2.2), a deep ocean conductivity-temperature-depth (CTD) sensor (6.2.3), a sampling device for nano- and micro-plastics (subtask 6.2.4), a low-cost microplastics fluorescence sensor (subtask 6.2.5), and a radioactivity sensor, which were described in WP4 Deliverables 4.1, 4.2, 4.3, 4.4, 4.5, and 4.7, respectively. These instruments were integrated onto various observing platforms as part of WP5 and will be deployed on field demonstrations and use cases in WP7. Calibration and validation of instruments reported here include tests performed in the laboratory or field stations using various standard solutions and materials (including some certified reference material, where relevant) and reference instruments, at times under realistic measurement scenarios to confirm proper operations *in situ* - e.g., pressurised to test maximum depth of operation, submerged in large test tanks, various temperature/salinity conditions, etc.
The calibration and validation of the radioactivity sensor (task 4.6) was not foreseen in the Grant Agreement, but nevertheless this has been carried out to support the sensor in the future demonstration phase. The calibration and validation of the radioactivity sensor was therefore reported in this deliverable.

II. OBJECTIVES

The main objective of these calibration/validation tests described in D6.2 was to characterise accuracy of measurements under real-world conditions and ranges as well as reliability of the instrument to make measurements according to the needs and requirements of demonstrations in WP7. Additional links with WP5 are also considered for some sensors to ensure that the instruments perform according to requirements when integrated with an observing platform. Improving the technical readiness level (TRL) was a key part of T6.2 activities in order to bring TRL to a level that will increase chances of successful in situ demonstrations.

III. LABORATORY TESTS

1. CARBONATE SYSTEM / OCEAN ACIDIFICATION SENSORS

Carbonate system sensors were calibrated with different calibration materials (reference measurements, calibration gases) and laboratory tests were performed in a large 1000 L tank with variable carbonate system conditions and seawater temperature to validate the performance of three “off-the-shelf” carbonate system sensors. Each sensor was paired with additional hardware and electronics, developed during NAUTILOS activities in WP4 and WP5, that were designed to improve sensor performance and usability at a reduced cost to the end user. A Honeywell Ion Sensitive Field Effect Transistor (ISFET)-based Durafet non-glass pH electrode (hereafter Durafet), an Endress-Hauser ISFET-based CPS77E pH electrode (hereafter Endress), and a Franatech membrane-based CO_2 sensor (CO2-SENSOR HR, hereafter CO2-HR) were selected (e.g., Honeywell ISFET pH sensor with pressure housing show in Fig. 1). These sensors allow users to measure 2 of the 5 measurable carbonate system parameters. Once any two of these 5 parameters are known, the rest of the system can be calculated assuming knowledge of salinity, temperature, and pressure. A benefit of measuring pH and the partial pressure of CO_2 (pCO_2) is that: 1) the measuring approach is relatively straightforward, 2) both measured parameters have direct use in industrial and marine science applications, and 3) high-temporal resolutions can be achieved when sampling both in situ and in an underway/flow-through system.

Figure 1: NAUTILOS Honeywell ISFET sensor with pressure housing.

1.1. Objectives

The specific goal for the Durafet and Endress ISFET pH sensor test was to calibrate and validate its performance relative to reference calculations of pH on the total hydrogen ion scale. Bresnahan et al. (2014) state that the Durafet is capable of accuracy, relative to a chosen reference, of better than 0.03 pH units over multiple months. However, the accuracy of the sensor time-series can be no better than the reference to which it is calibrated or validated. According to the Measurement Quality Goals for the Global Ocean Acidification Observing Network (GOA-ON), "Climate" quality measurements are to have an uncertainty of ±0.003 or better, and "Weather" quality measurements are to have an uncertainty of ±0.02 pH units or better. Therefore, the objective of this test is to achieve "Weather" measurement standards, which are measurements of sufficient quality to identify relative spatial patterns and short-term variation. With respect to ocean acidification, this will support mechanistic interpretation of ecosystem response and impact on local, immediate ocean acidification dynamics (Newton et al., 2015).

The specific goal for the CO2-HR pCO_2 test was to calibrate the sensor with gas standards through the end cap and validate its performance relative to discrete samples of calculated pCO_2 (described in Section 1.2) and other membrane-based pCO_2 sensors. The CO2-HR sensor, in its default configuration, cannot easily be re-calibrated by the user (there is no direct access to the gas analyser inside). To overcome this, activities in NAUTILOS developed an end cap that fits over the outside of the membrane. Calibration gases and seawater can be alternately pumped through the cap, which enables the detector to be calibrated and the sensor to be configured for flow-through operation. The manufacturer states that a feature of the CO2-HR sensor is "reliable and accurate values 1-50 mg/L" (equivalent to ~516-25,800 ppm), and that it is suitable for: 1) process control in aquaculture, 2) long-term monitoring in hydroelectricity reservoirs, and 3) surveys of coastal waters. No accuracy data is provided by the manufacturer. The GOA-ON "Weather" quality measurements have been assigned an uncertainty of 2.5%, while the "Climate" quality measurements are 0.5%.

1.2. Calibration and validation references

To validate measurements from both pH and pCO_2 sensors, seven discrete samples of dissolved inorganic carbon (DIC) and total alkalinity (TA) were collected throughout the experiment, poisoned with a saturated solution of mercuric chloride, and analysed on a VINDTA according to the "gold-standard" procedures outlined in Dickson et al. (2007). Routine analyses of Certified Reference Material from Scripps Institution of Oceanography were used to verify that measurement accuracy

and precision for DIC and TA analyses were better than ±2 µmol kg^{-1}. These samples, along with phosphate and silicate, measured using the methods outlined in Grasshoff et al. (1999), as well as temperature and salinity, were used to calculate pH and pCO_2 using the MATLAB program *CO2SYS.m* (Lewis & Wallace 1998; van Heuven et al., 2011). The carbonic acid dissociation constants of Mehrbach et al. (1973) refit by Dickson and Millero (1987) were used, along with the bisulfate constant of Dickson (1990) and the boron/salinity ratio of Uppström (1974). Uncertainties of calculated values were estimated by propagating the uncertainties of each input variable with the MATLAB program *errors.m* (Orr et al. 2018). This resulted in an average pH and pCO_2 uncertainty of ±0.008 and ±21 µatm, respectively.

The calibration of pH sensors followed the procedure outlined by Bresnahan et al. (2014) and used voltage/pH data from the electrode and a single point calibration. In these tests, both pH sensors were calibrated to the calculated pH value of the first bottle sample. The CO_2 sensors used in the test were calibrated with standard gases: nitrogen (zero pCO_2), and up to 5 concentrations of pCO_2-in-air (200, 400, 802, 2000 and 4010 ppm; Fig. 2). Gases were provided by Linde Industrial Gases. The mole fractions of CO_2 (xCO_2) were converted to pCO_2 at in-situ water temperature and 100% humidity by using the equations of Weiss (1974) and Takahashi et al. (1993). Additional CO_2 sensors, used for comparative purposes, included the subCtech OceanXpert-Lab IR-CO2 flow-through analyzer (hereafter OceanXpert-Lab) and the subCtech OceanXpert-Sea IR-CO2 subsea analyzer (hereafter OceanXpert-Sea) with a manufacturer-claimed accuracy of <0.5%. Temperature and salinity of the test tank was measured using a flow-through Sea-Bird SBE 45 thermosalinograph and an in situ SBE 38 digital oceanographic thermometers (accuracy ±0.003°C).

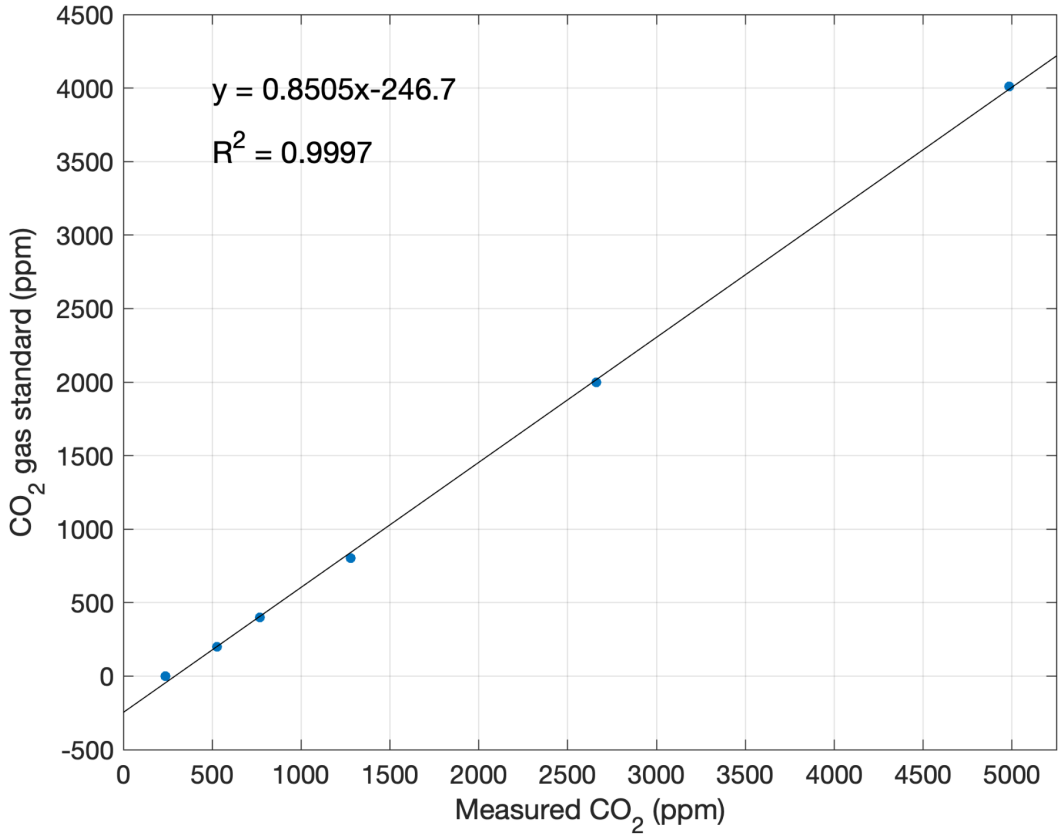

Figure 2: Calibration coefficients for the CO2-HR sensor. Gas standards were pumped through the end cap enclosing the membrane until equilibration across the membrane had occurred.

1.3. Description of the tests

This validation exercise assessed the response time and compared measurement output of NAUTILOS pCO_2 and pH sensors by manipulating the carbonate chemistry and temperature inside a 1000 L tank of seawater over a 24-hour period. Carbonate chemistry was altered via three incremental additions of 100 ml 1N hydrochloric acid (HCl) and five incremental additions of 100 ml 1N sodium hydroxide (NaOH). The R package *seacarb* (Gattuso et al., 2021), specifically the functions *ppH.R* and *carb.R*, were used to estimate the required additions of acid or base to keep seawater carbonate chemistry manipulations within the measurement/detection range of all sensors. Temperature was changed with the use of a low-temperature heating element. Bottle samples for reference measurements were collected just before the various acid/base additions.

1.4. Results

The results of the validation experiments for pH and pCO_2 are shown in Figs. 3 and 5 and Tables 1 and 2, respectively. For the pH validation experiment (Figure 3 and Table 1), the Durafet and Endress ISFET pH values were single-point calibrated according to Bresnahan et al. (2014) at the 00:02:00 elapsed time point at the start of the experiment. The successive pH adjustments, as described in Section 1.2, are evidenced by the step increase and decrease in measured pH. This, along with the gradual changes in seawater temperature create a diverse set of pH and temperature pairs. Inspecting the response time of pH sensors after the first acid addition shows a t90 response time, the length of time measurements take to reach 90% of their final value, of ~4 minutes each (Fig. 4). While the differences between pH measurements and CO2SYS calculated pH ranged from ±~0.002 at the second and third sampling points, the delta values increase to +~0.3-0.6 at the end of the experiment, which possibly indicates the need for long-term conditioning of ISFET electrodes at seawater ionic strength (Bresnahan et al., 2014). Electrodes in this study were conditioned in seawater for several days, but a conditioning period of several weeks might be required and will be further investigated. Regardless, the mean absolute error for both the Durafet and Endress ISFET pH sensors were 0.028 and 0.023 (Table 1), respectively, which is in line with the objective of "Weather" measurement standards cited in Section 1.1 (±0.02 pH) and is also a reasonable level of uncertainty for use with aquaculture and citizen science applications.

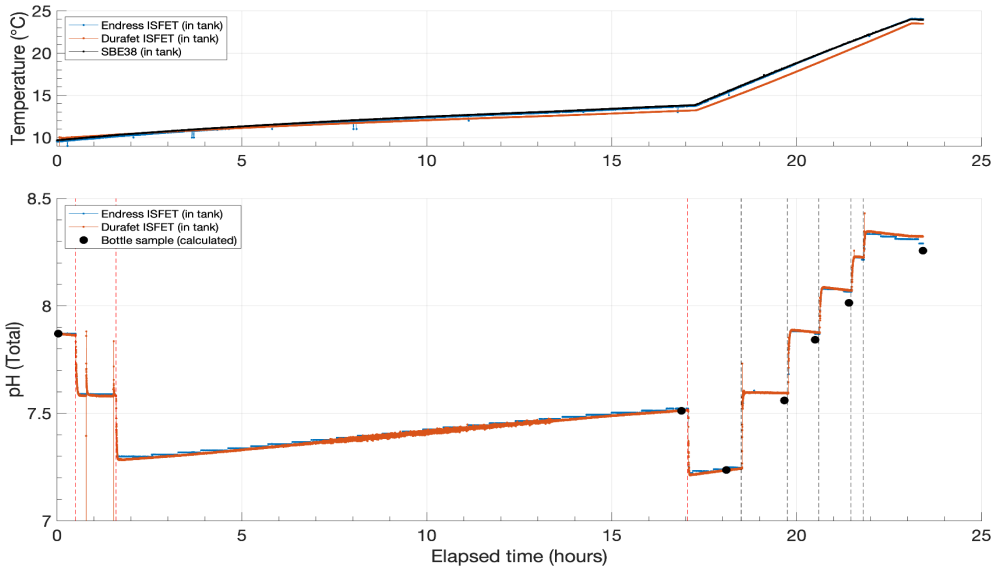

Figure 3: pH values during ~24-hour in-tank test. Top panel shows temperature values from inside each sensor and reference temperature at in situ conditions (SBE38). Bottom panel shows pH values at in situ temperature, red dashed lines indicate timing of acid addition.

Table 1: pH values at in situ temperature. Both Durafet and Endress electrodes were calibrated to the first bottle sample. Mean absolute error (MAE), relative to bottle samples, is calculated for each ISFET sensor.

Elapsed time	pH bottle sample (calculated)	pH Durafet ISFET	pH Endress ISFET
0:02:00	7.871 ± 0.009	7.871	7.871
16:53:00	7.511 ± 0.011	7.514	7.522
18:06:00	7.236 ± 0.01	7.234	7.239
19:40:00	7.56 ± 0.011	7.595	7.593
20:30:00	7.842 ± 0.008	7.878	7.870
21:25:00	8.014 ± 0.006	8.071	8.066
23:25:00	8.257 ± 0.004	8.322	8.290
MAE	*0.008*	*0.028*	*0.023*

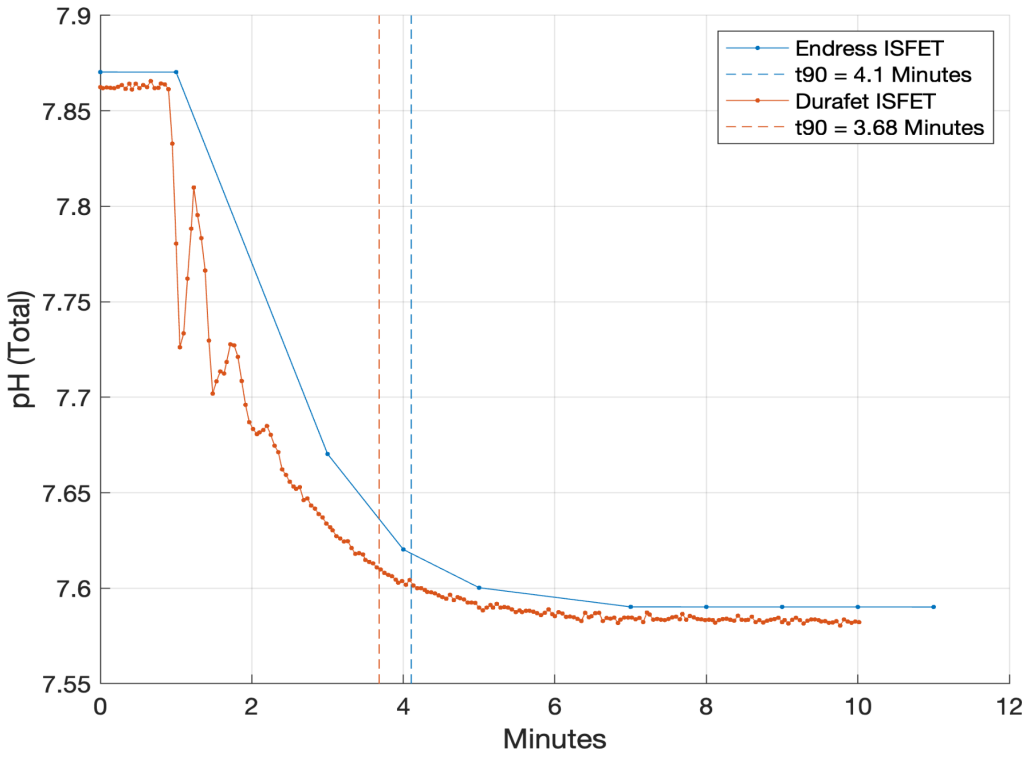

Figure 4: Response time of pH sensors after first acid addition. Dashed lines indicate how long measurements from each sensor take to reach 90% of the final value (t90).

The pCO_2 validation test results also exhibit similar step increase and decrease with each manipulation of carbonate chemistry (Fig. 5, Table 2). The steps are smoother for pCO_2 measurements in comparison with pH measurements primarily due to the membrane equilibration systems that all three sensors employ - CO_2 in the sensor detection loop must be flushed out and equilibrated with the new higher or lower pCO_2 from seawater. The t90 response times show that this equilibration time is decreased when the membrane equilibration systems are in a pumped/flowthrough system and ranged from ~10-45 minutes (Fig. 6), which was significantly longer than for pH t90 response times. In this test, the OceanXpert-Sea was not actively pumped and showed a t90 response time of ~45 minutes, relative to the ~12-20 minute t90 response time of the pumped/flow-through systems.

In the case of pCO_2 measurements, the reference pCO_2 values for validation experiments is not well defined and the mean "consensus" value is often used as a reference value (ICOS-ERIC, pers. comm.). In this test, we have not assigned a reference value, but instead evaluate the pCO_2 measurements as a group and also include CO2SYS calculated pCO_2 at each measurement time point. However, it has been acknowledged that calculated pCO_2 is dependent on a number of inputs and constants which can lead to bias depending on how well constrained the carbonate system and water conditions are. That said, all three pCO_2 sensors increased and decreased according to the expected direction of change. The NAUTILOS-developed CO2-HR sensor had a mean absolute error of ±74 µatm relative to the bottle sample calculations (Table 2). In regard to the "Weather" objective cited in Section 1.1, a relative uncertainty of 2.5% is the "Weather" objective for pCO_2, which translates to 10 ppm at 400 µatm pCO_2, 25 µatm at 1000 µatm pCO_2, and 75 µatm at 3000 µatm pCO_2. When used for applications related to citizen science and aquaculture, the "Weather" objectives are more than adequate when examining seasonal variability in coastal systems where natural pCO_2 variability can be very high and in aquaculture scenarios where qualitative but reliable measurements are desired (i.e., when assessing safe levels for finfish physiology).

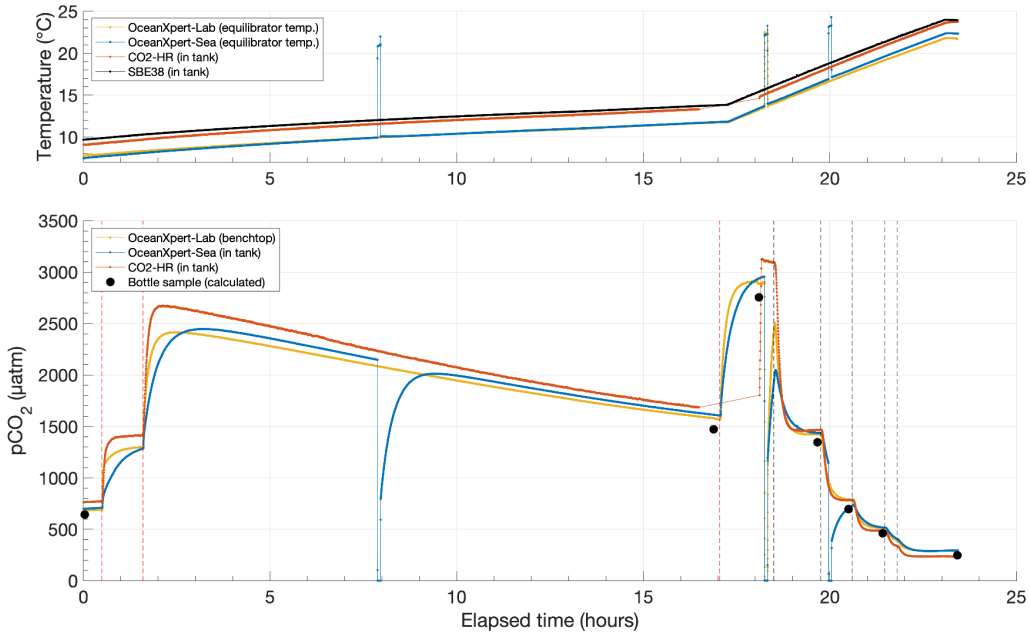

Figure 5: pCO_2 values during ~24-hour in-tank test. Top panel shows temperature values from inside each sensor and reference temperature at in situ conditions (SBE38). Bottom panel shows pCO_2 values at in situ temperature, red dashed lines indicate timing of acid addition.

Table 2: pCO_2 (µatm) values at in situ temperature. Mean absolute error (MAE), relative to bottle samples, is calculated for each sensor.

Elapsed time	pCO_2 bottle sample (calculated)	pCO_2 CO2-HR	pCO_2 OceanXpert-Lab	pCO_2 OceanXpert-Sea
0:02:00	644 ± 12	765	685	700
16:53:00	1474 ± 34	-	1580	1613
18:06:00	2756 ± 55	-	2889	2939
19:40:00	1346 ± 29	1469	1424	1437
20:30:00	697 ± 12	785	790	706
21:25:00	461 ± 6	486	515	518
23:25:00	248 ± 2	233	291	296
MAE	*21*	*74*	*78*	*83*

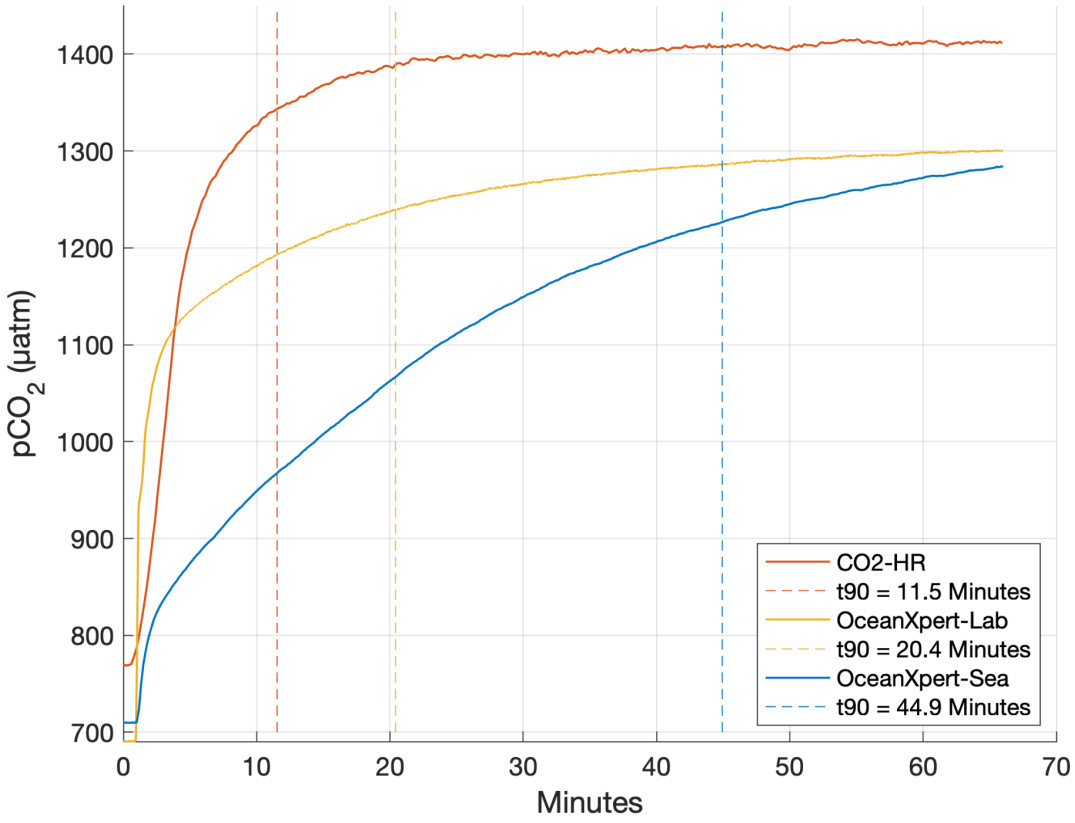

Figure 6: Response time of pCO_2 sensors after first acid addition. Dashed lines indicate how long measurements from each sensor take to reach 90% of the final value (t90).

2. SILICATE SENSOR

The electrochemical silicate sensor (new optimised design) presented on Fig. 7 is an anodized aluminium cylinder of 9 cm diameter and 25 cm long with a weight of 2.2 kg. The electronics, placed into a dry compartment, control the whole analytical procedure and store data. The optimum response time of the sensor is around 15 minutes with 10 seconds devoted to sampling seawater.

Figure 7: Optimised design of Silicate in situ electrochemical sensor.

Silicates are non-electroactive species and therefore are detected indirectly by electrochemistry after complexation with molybdates at acidic pH. The reagents are produced by oxidising a molybdenum electrode at 1,5 V/Ag/AgCl/Cl- (0,6M) according to Eq. 1. The counter electrode (titanium grid) is isolated behind a 180 µm Nafion® membrane (N117 Du Pont™ Nafion® PFSA Membrane) to avoid the reduction of H^+ formed into H_2 and therefore to obtain acidic pH required. A chlorinated silver rod is used as a reference electrode for this step.

$$Mo + 4H_2O \rightarrow MoO_4^{2-} + 8H^+ + 6e^- \quad \text{(Eq. 1)}$$

The silicomolybdic complex formed (Eq. 2) is then detected by square wave voltammetry using a conventional three-electrode system (disc ϕ =2 mm) with gold working electrode, silver electrode covered with silver chloride layer as reference electrode and platinum as counter electrode.

$$Si(OH)_4 + 12\,MoO_4^{2-} + 24\,H^+ \rightarrow H_4Si(Mo_{12}^{(VI)}O_{40}) + 12\,H_2O \quad \text{(Eq. 2)}$$

The gold electrode must be cleaned before its use with mechanical abrasion and electrochemical cleaning in H_2SO_4 (0.5 M). This modifies the electrode's surface, and it is therefore necessary to re-calibrate the sensor after each cleaning and before each deployment/use of the sensor.

An example of calibration is presented in the following pages.

2.1. Objectives

The objectives are to calibrate the silicate sensor using standards diluted in artificial seawater in the concentration range observed in the open ocean (0 - 140 µM) and to validate the calibration obtained using real seawater samples with precise and known concentrations of silicate.

2.2. Calibration and validation references

Silicate standards for calibration

A commercial silicate standard solution SiO_2 of 1017 mg L^{-1} ± 9 mg L^{-1} (16926 ± 150 µM) was used to prepare diluted standards in artificial seawater made with 32.74 g of NaCl, 7.26 g of $MgSO_4$, $7H_2O$ and 0.172 g $NaHCO_3$ in 1 L MilliQ water at pH ≈ 8 and salinity close to 35 psu (Table 3)

Table 3: The concentrations of the standard solutions analysed with the silicate sensor and their standard deviations (SD).

$[Si]_{standards}$ ± SD (µM)
1.69 ± 0.17
2.54 ± 0.17
4.23 ± 0.42
6.77 ± 0.43
8.46 ± 0.43
15.2 ± 0.2
33.9 ± 0.3
50.8 ± 0.5
84.6 ± 0.8
101.6 ± 0.9

Certified Reference Materials for accuracy evaluation

In order to evaluate the accuracy of the results obtained with the sensor, several Certified Reference Materials (CRM) supplied by KANSO CO. LTD. Japan were analysed. Silicate concentrations given by the supplier with respective standard deviation (SD) and expanded uncertainty, as well as salinities and densities are gathered in the Table 4.

Table 4: CRM composition (only silicate concentrations are indicated but samples contain phosphate, nitrate and nitrite as well).

	Certified value ± SD (µmol kg^{-1})	Expanded uncertainty (µmol kg^{-1})	Salinity (psu)	Density (20°C)	$[Si]_{CRM\_ref}$ (µmol L^{-1})
Lot. CL	13.8 ± 0.012	0.3	34.685	1.0245	**14.1**
Lot. CO	34.72 ± 0.021	0.16	34.282	1.0242	**35.56**
Lot. CP	61.1 ± 0.035	0.3	34.398	1.0243	**62.6**
Lot. CM	100.5 ± 0.052	0.5	34.414	1.0243	**102.9**
Lot. CN	152.7 ± 0.095	0.8	34.536	1.0244	**156.4**

2.3. Description of the tests

For all the experiments made in the laboratory, the sensor was equipped with a funnel in order to fill the electrochemical cell with silicate standards and CRM solutions, while the sensor was immersed in ~40 L tank of artificial seawater (Fig. 8).

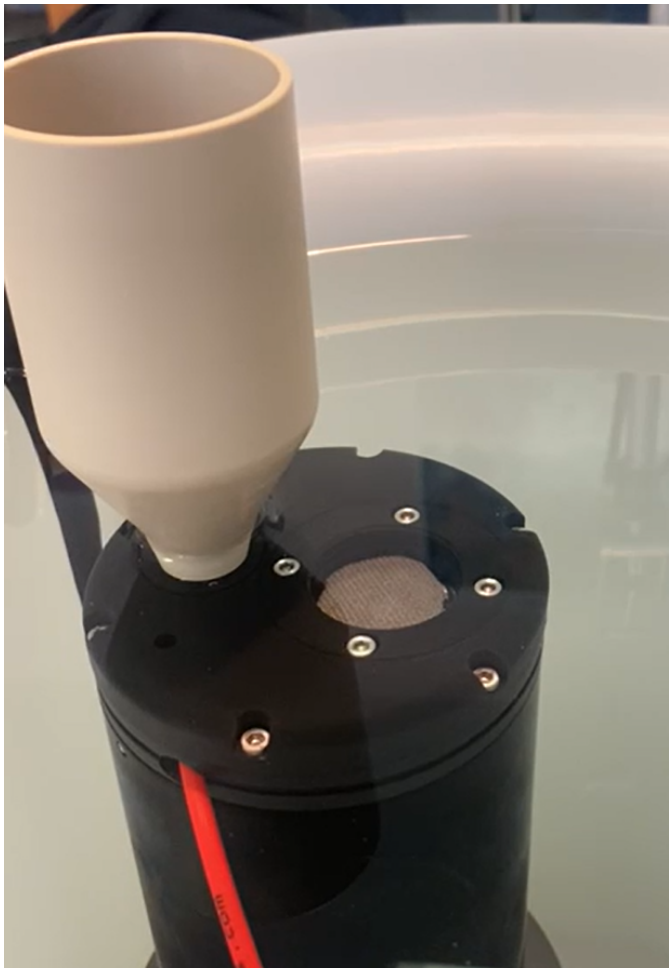

Figure 8: Silicate sensor equipped with funnel for laboratory experiments immersed in artificial seawater tank.

Calibration

The calibration procedure consisted of filling the silicate sensor via the funnel with artificial seawater solutions containing silicate concentrations ranging from 1.69 to 101.6 µM while the silicate sensor was immersed in a 40 L tank of artificial seawater, and recording the square wave voltammograms of each solution.

The differential current in microamperes is then plotted against the scan potential applied on the gold working electrode. The voltammograms obtained are finally post-analysed using NOVA software (Metrohm®) in order to measure the peak differential intensity corresponding to silicomolybdic complex reduction.

Accuracy test

To evaluate the accuracy of the results as well as to certify the calibration, Certified Reference Material (CRM) were analysed by the sensor. These CRMs were stabilised, real seawater samples with known silicate concentrations. The procedure is the same as the calibration: square wave voltammograms are recorded for CRM with the sensor. Peak differential intensities are measured via NOVA software

and silicate concentrations are determined using the calibration made and values obtained are compared with reference values to determine accuracy of the sensor.

2.4. Results

Calibration

Calibration plots correspond to the peak intensities versus reference silicate concentrations in solution. An example is given in Fig. 9. As previously reported in D4.2, a shift in slope was observed when silicate concentration greater than ~15 µM was measured, indicating different mechanisms of reduction according to silicate concentration. Depending on the peak intensity measured, the appropriate equation will be used to determine silicate concentration.

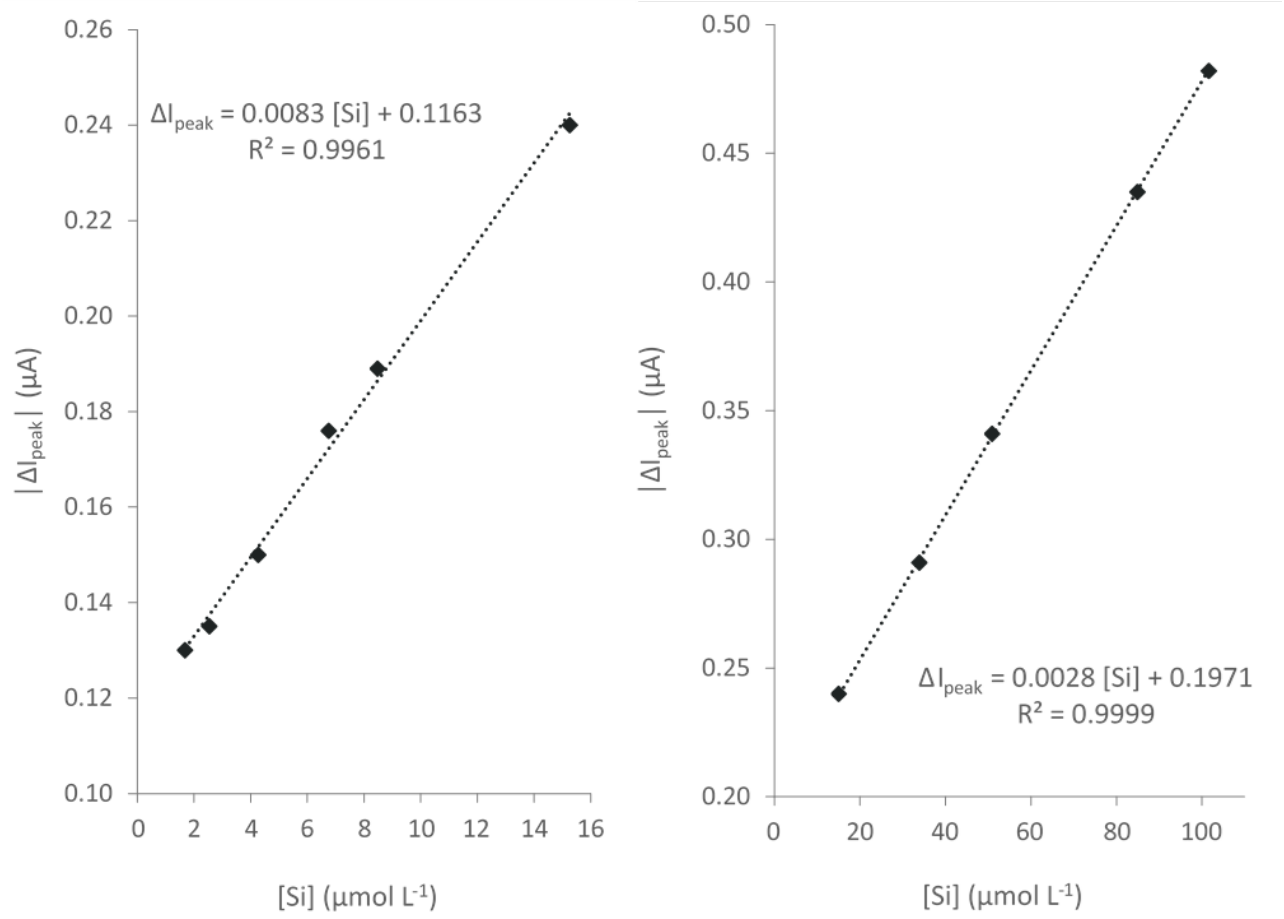

Figure 9: Calibration plots of silicate standards obtained with the electrochemical sensor.

Accuracy

In order to certify the calibration and values obtained, 5 different lots of CRM were analysed by the sensor. The results obtained are presented in the following Table 5 showing good accuracy under 2% where accuracy is defined by the Eq. 3. Results are also compared with the calibration curve obtained in Fig. 10, illustrating the accuracy of the silicate sensor.

$$Accuracy = \frac{|[Si]_{exp} - [Si]_{CRM\_ref}|}{[Si]_{CRM\_ref}} \ (\%) \qquad \text{(Eq. 3)}$$

Table 5: CRM analysis with silicate sensor and accuracy evaluation.

	$[Si]_{CRM\_ref}$ (µM)	$\lvert\Delta I_{peak}\rvert$ (µA)	$[Si]_{exp}$ (µM)	Accuracy (%)
Lot. CL	14.1	0.234	14.18	0.6%
Lot. CO	35.56	0.295	34.96	1.7%
Lot. CP	62.6	0.373	62.82	0.4%
Lot. CM	102.9	0.48	101.04	1.8%
Lot. CN	156.4	0.642	158.89	1.6%

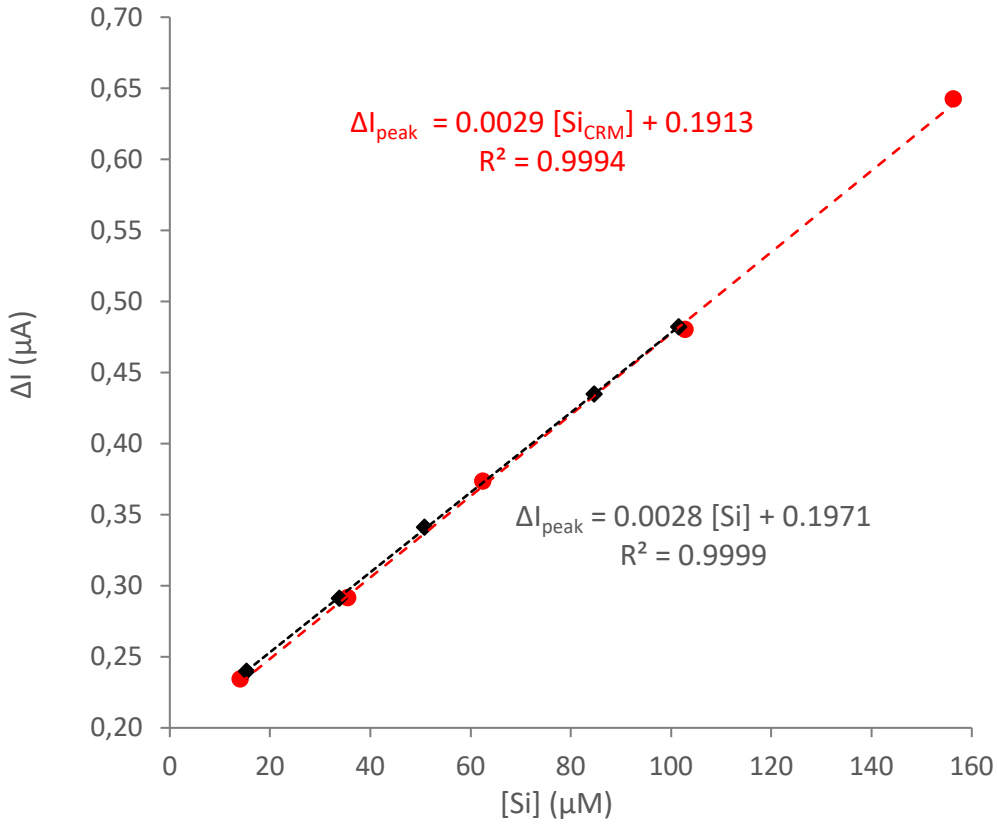

Figure 10: Calibration plot of silicate sensor compared with results obtained with CRM.

3. DEEP OCEAN CTD

Since the late 1960's, the electronic measurement of conductivity, temperature and pressure provided by the CTD (conductivity, temperature and depth) has become the backbone of hydrography and oceanographic measurements in the ocean. It is noteworthy that accumulated experience gained from using CTDs as essential equipment in marine observatories and oceanographic missions for more than half a century, along with the establishment of internationally recognized traceable standards for these parameters, has significantly improved their effectiveness compared to other measurement parameters. To ensure the highest data quality, calibration, procedures and adjustments must be applied to CTD sensors. It is generally accepted that the standard for temperature is a platinum resistance thermometer calibrated to fixed points of water that are traceable to the international standards for temperature (ITS-90) and for conductivity a high precision conductivity ratio bridge,

capable of an accuracy of at least 0.002 mS/cm in conductivity (equivalent to better than 0.003 in salinity) and resolution which is ten times better (Table 6). For pressure the standard is the pressure balance, also known as the piston gauge and deadweight tester (Table 6). The use of the pressure balance involves the manual placement of weights on the instrument together with an adjustment of the position of the piston. Although the primary standards for the calibration of the CTD sensors exist, there are limitations. For example, the dimensions and geometry of a CTD temperature sensor must allow its insertion into the fixed point cell, a feature which excludes most, if not all, CTD sensors used for oceanographic measurements to date. Thus, a laboratory transfer standard like a high precision thermometer or conductivity sensor must be employed in order to calibrate the CTD sensor. A satisfactory calibration can probably only be achieved by total immersion of the instrument rather than by immersion of the sensor alone. The requirement is thus for a well-regulated bath large enough to contain the CTD and calibration procedures that may differ from one laboratory to another.

Parameter	Conductivity	Temperature	Pressure
Sensor	Inductive Cell	Platinum Thermometer	Precision-machined Silicon
Range	0 - 7.0 S/m (0 - 70 mS/cm)	-2° to 35°C	Customer specified
Accuracy*	±0.0002 S/m (±0.002 mS/cm)	0.002°C	±0.01% full scale*
Stability	±0.00005 S/m/month (±0.0005 mS/cm/month)	±0.0002°C/month	±.002% full scale/month
Resolution	0.00001 S/m (0.0001 mS/cm)	0.00005°C	0.0004% full scale
Response	5.0 cm at 1 m/sec	150 msec Platinum 20 msec Thermistor**	25 msec

Table 6: ICTD WOCE Specifications source: salinometry.com

3.1. Objectives

A CTD instrument for deep ocean measurements was developed and initially tested by the University of Ljubljana -Faculty of Electrical Engineering for the Task 4.5: Deep-ocean CTD (Fig. 11). The NAUTILOS CTD comprises integrated MEMS-based Au thin film electrode conductivity cell and thin film Ti temperature sensor on the common substrate (CT chip), a separate OEM Keller pressure sensor and electronic circuitry for control and signal processing, all assembled in a watertight pressure resistant SS 316L housing suitable for deep sea environment (UL FE design). All three sensors were packaged in two openings in the top cover of the CTD housing. The CT chip is first attached by epoxy glue in a SS case, fitting to one of two watertight ports of the metal housing. The pressure sensor is mounted into the second port of the top cover, with connecting wires extending downwards to PCB inside the SS cylindrical body. Both sensors as well as the electrical connector and front- and back- cover plate are sealed with Viton® O-rings on the cylindrical body. The watertight SS 316L cylindrical housing accommodates the PCB of CTD electronic circuitry, fastened to the front cover of the CTD housing and all necessary connections to the sensors and outside connector. Software provides the algorithms protocol for each sensor with calibration coefficients and data acquisition scenarios. The back cover plate contains an underwater connector for communications and power supply. Data are recorded in the instrument memory and are simultaneously available through RS-232 I/O watertight connector pins. The whole system has a diameter of 120 mm and a length of 300 mm.

Initial tests of the NAUTILOS CTD performance were carried out in the University of Ljubljana -Faculty of Electrical Engineering laboratories during the development phase of the instrument (ref D4.1). The tests were performed using professional laboratory instruments and an OEM electronics evaluation kit AD CN0359 aiming to characterise the sensing elements and the final assembled CTD unit with the electronics. The specifications of NAUTILOS CTD sensor are summarised below in Table 7.

Figure 11: NAUTILOS Deep Ocean CTD instrument.

Table 7: Specifications of the NAUTILOS CTD instrument.

Parameter	***Range***	***Accuracy***	***Sensitivity***
Temperature	*2 °C - 40 °C*	*> 0.05 °C*	*>0.01 °C*
Conductivity	*4-70 mS/cm*	*> 0.1 mS/cm*	*> 0.01 mS/cm*
Pressure (OEM)	*0…200 bar*	*±0.5 %FS*	**0.85 mV/bar*

**data from Keller*

The work was carried out in the POSEIDON Calibration laboratory (PCL-https://poseidon.hcmr.gr/components/supporting-facilities/calibration-lab) at the Hellenic Centre of Marine Research (HCMR) Thalassocosmos complex in Crete between 7 - 14 of June 2023. The lab tests and calibrates sensors for a range of oceanographic parameters focusing on the unique environmental conditions of the Eastern Mediterranean sea. The objective of the Sub-task 6.2.3 reported here, following the work done during the development task, was to perform calibration experiments and compare the sensor data against the measurements of the laboratory reference instrumentation in order to:

- apply a temperature correction coefficient for the NAUTILOS CTD temperature sensor in a predefined temperature range corresponding to realistic environmental conditions
- apply a conductivity correction coefficient for the NAUTILOS CTD conductivity sensor cell in a predefined conductivity range corresponding to realistic environmental conditions

3.2. Calibration and validation references

Description of equipment

The PCL calibration tank has a cylindrical shape, with an inner diameter of about 122 cm and an inner height of 120cm, allowing all the temperature/conductivity measuring instruments to be fully

immersed in it (Fig. 12). The tank is made of PVC walls and polyurethane filling, and the 9-cm thick walls provide excellent heat insulation. It is equipped with a 6000 W heating element and an electric motor equipped with a propeller for the efficient homogenization of the water in the tank.

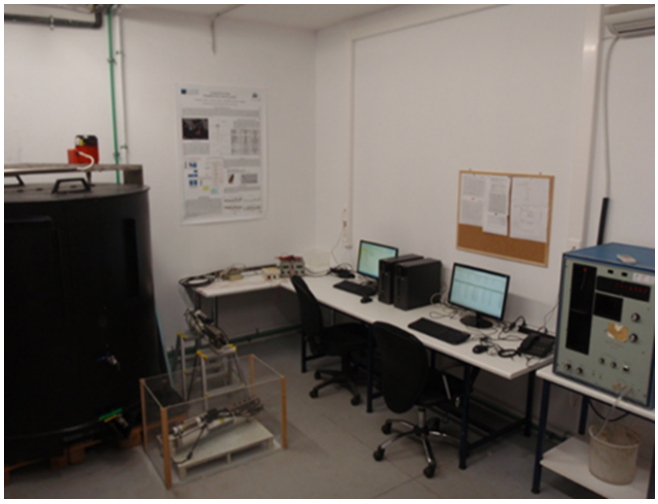

Figure 12: The Poseidon calibration laboratory. The black calibration tanks to the left side of the picture.

At a height of about 92 cm from the bottom of the tank, there are two metal brackets for the deployment of the various sensors to be calibrated. The two brackets also mark the minimum level at which the heater of the tank should be operated. This level amounts to about 1.1 m^3 of water, considering a horizontal surface of 1.17 m^2 of the interior of the tank. In order to develop an operating protocol for the T/C calibration tank, we performed several tests using combinations of heating and mixing possibilities. The thermal response of the tank was recorded using a Seabird SBE35 thermometer. An example of the heating rate of the tank is presented in Fig. 13 below.

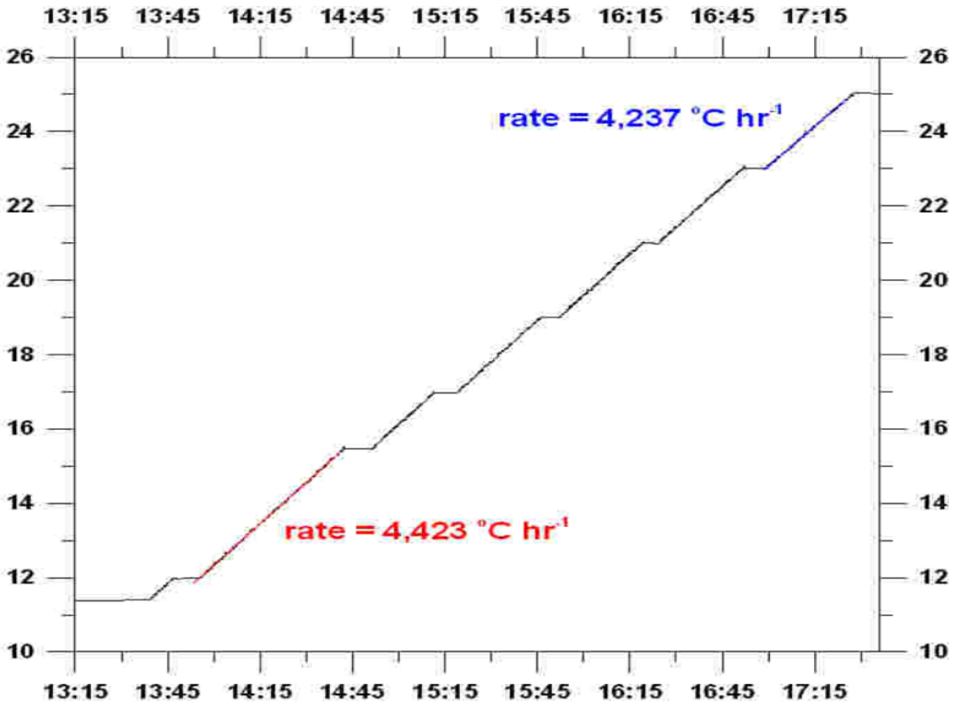

Figure 13: Rate of temperature increase inside the PCL calibration tank. At times when the temperature appears to remain constant, the heater has been turned off in order to proceed to sampling for calibration. The red and blue lines denote fits to the heating rate performed at about 14:00-14:45 and 17:00-17:20, respectively. The maximum heating rates are estimated to about 4.3±0.2 °C hr^{-1}.

Reference instrumentation

The temperature reference sensors used in the HCMR calibration lab are the SBE 35 Deep Ocean Standards Thermometer manufactured by Seabird Electronics with an accuracy of ± 0.001 °C and stability of 0.001 °C per year (http://www.seabird.com/products/spec_sheets/35data.htm). For conductivity measurements we use as secondary reference a SBE 37SIP with an accuracy of ± 0.0003 S/m (http://www.seabird.com/moored/sbe-37-si-and-sip-microcat/family-downloads?productCategoryId=54627473785). The reference instruments of the PCL (Table 8) are calibrated against primary standards in certified laboratories.

Table 8: Details of the reference instrumentation are shown.

Parameter	Model	S/n	Accuracy	Stability
Temperature	*SBE 35*	*0058*	*0.001°C*	*0.001°C per year*
Temperature	*SBE 35*	*0059*	*0.001°C*	*0.001°C per year*
Conductivity	*SBE 37SIP*	*5272*	*0.0003Sm^{-1}*	*0.0036 Sm^{-1} per year*

Calibration uncertainty

The temperature uncertainty budget consists of three components: tank stability, tank homogeneity and reference thermometer accuracy. Guide to the expression of Uncertainty in Measurement (GUM) was used for the calculation of the uncertainty components and their combination. Tank stability and homogeneity were estimated from the readings of the reference thermometers at each "window" (type A). Reference thermometer uncertainty was estimated from the specifications of the thermometers (type B). The expanded uncertainty, with a coverage factor k=2, of the reference temperature sensors is ±0.0034 °C (Table 9).

Table 9: The components of the uncertainty budget of the temperature calibration are shown.

Source	Manufacturer's specification	Assumed probability	Observed	Standard uncertainty
Temperature bath stability	-	-	*0.0009°C*	*0.0009°C*
Temperature bath homogeneity	-	-	*0.0012°C*	*0.0012°C*
Reference thermometer stability	*0.001°C y^{-1}*	*Rectangular*	-	*0.0006°C*
Reference thermometer accuracy	*0.001°C*	*Rectangular*	-	*0.0006°C*
Combined standard Uncertainty				*0.0017°C*
Expanded uncertainty (k=2)				*0.0034°C*

3.3. Description of the tests

Calibration procedure

The aim is to produce predefined calibration steps at regular intervals with an achieved homogeneity of the seawater mass inside the calibration tank. Seawater is collected one day prior to the calibration stored in a freezing chamber and the temperature calibration procedure begins with the lowest

temperature of the range selected. The period of time at which useful data are collected is a “window”. The cycle of heating/stirring, settling and actual measuring is a “step”. Data is collected via software for programming and logging (Fig. 14).

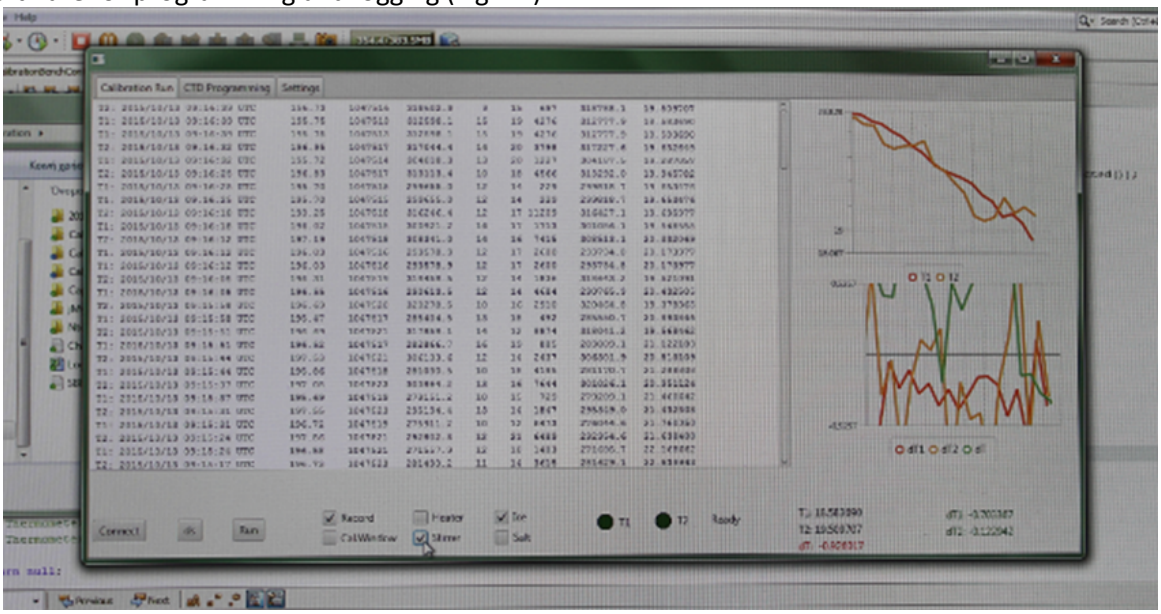

Figure 14: A snapshot of the software developed to facilitate the programming of the CT sensors, the upload and analysis of the data collected and to provide real-time monitoring of the calibration procedure.

During the experiment the temperature reference sensors and the NAUTILOS CTD were placed at the same water level using the tank brackets and supporting ropes and both sensors were programmed to start at the same time (Fig. 15). Sampling frequency was set to 1Hz for the temperature reference sensor and polled sampling commands were used for the NAUTILOS CTD.

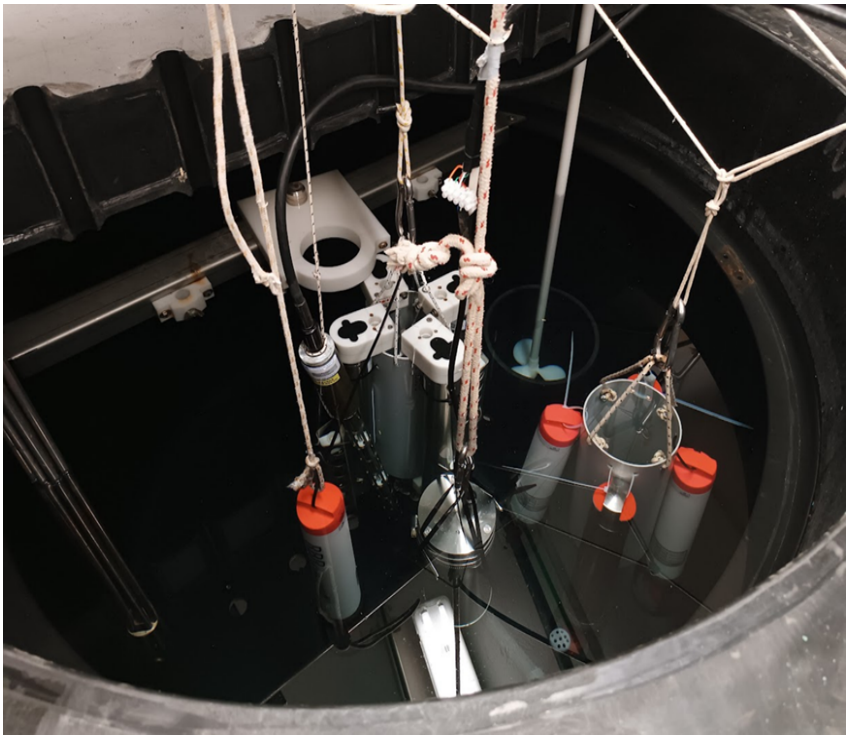

Figure 15: The NAUTILOS CTD and other RBR CT sensors placed inside the PCL calibration tank.

Successive “steps” were performed at progressively higher temperatures. The stirrer was used to homogenise the tank at each “step” and then the stirrer was turned off and the tank was given sufficient time to equilibrate. Real-time monitoring (Fig. 16) of the reference readings was used to decide start and end points of the calibration “window” of each step and high frequency data are collected. After the completion of a “step” the heater and stirrer were turned on to increase the temperature of the tank to the value of the next “step”. The procedure is fully controlled as shown in Fig. 16. The 9 calibration “steps” of the temperature calibration experiment ranged from 14.2°C to 22.9°C.

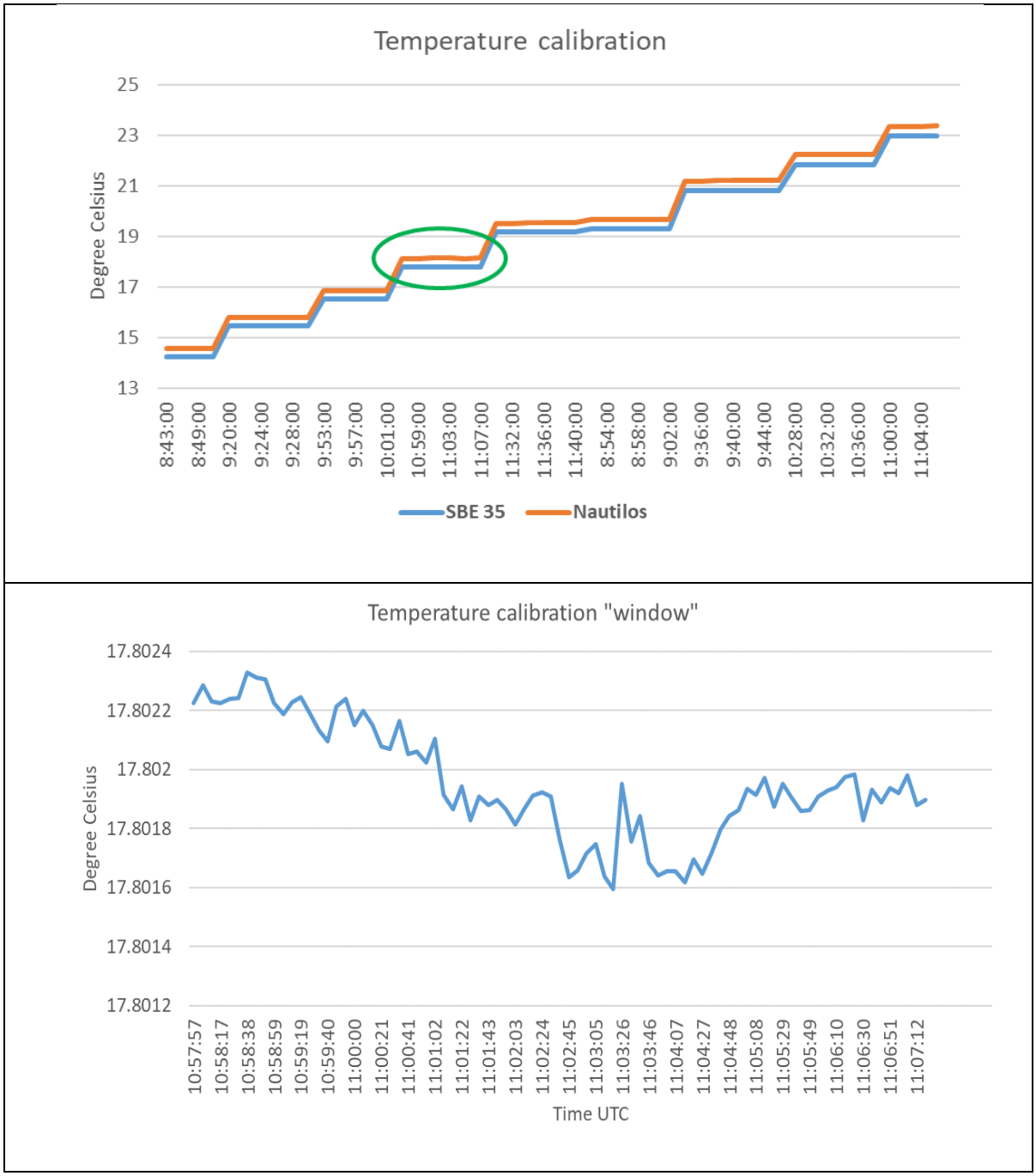

Figure 16: The temperature calibration timeseries is presented in the upper panel. The panel below corresponds to the calibration window highlighted by the green oval.

The calibration of the conductivity sensor was performed after the temperature calibration and a SBE 37 sensor was placed inside the tank to provide conductivity data for the experiment. The sampling

interval of the conductivity sensor was set to 15 sec. For the conductivity experiment we gradually remove the seawater and replace it with freshwater with similar temperature in order to decrease the conductivity to the lower point of the selected range (Fig. 17). The reference sensor was the SBE 37 and data inside the calibration "window" were used for the evaluation of the sensors and the calculation of new coefficients. The experiment was performed at the conductivity range of 5.82 S/m to 3.06 S/m while the temperature ranged from 24.74 °C to 24.35 °C.

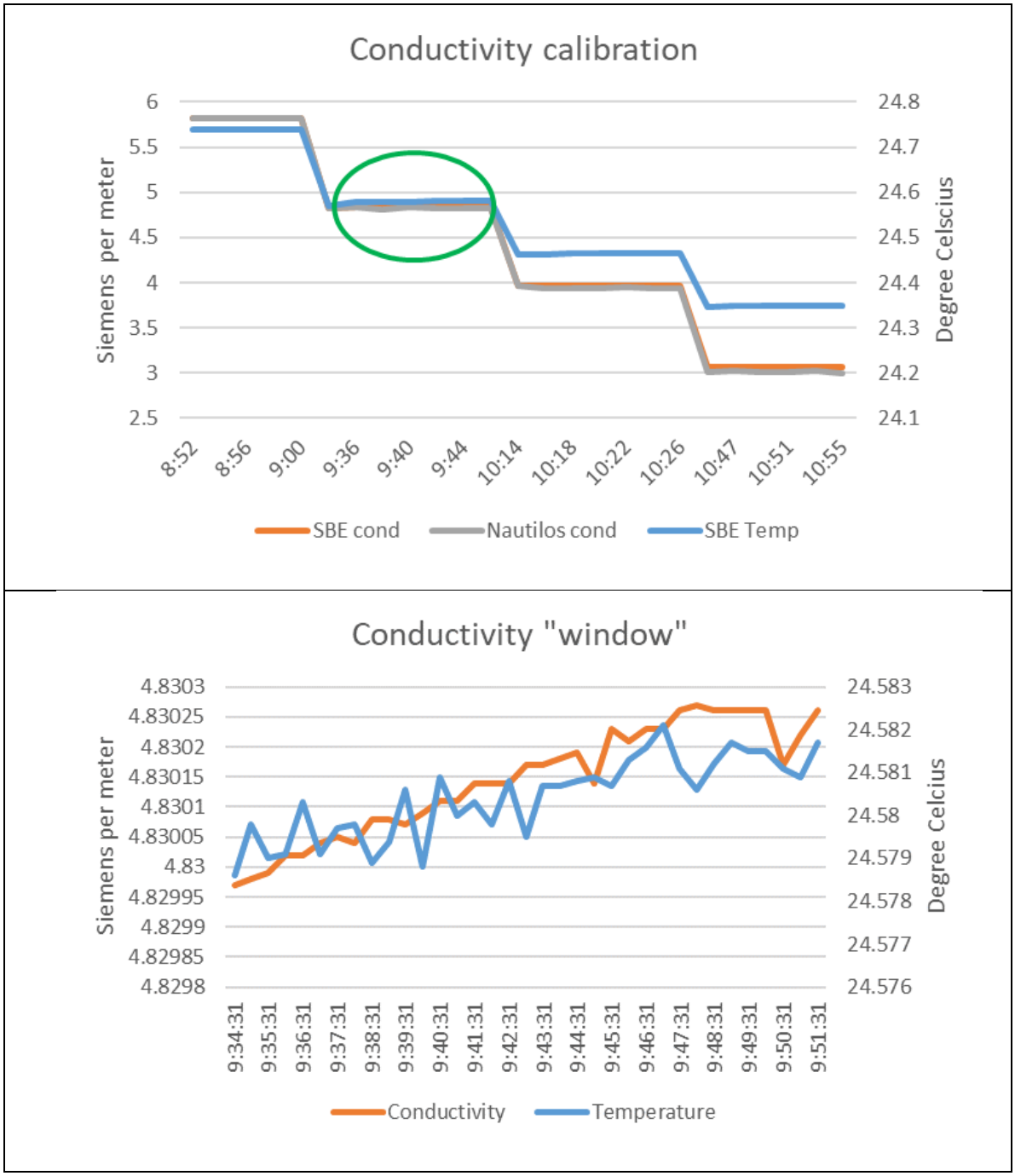

Figure 17: The conductivity calibration timeseries is presented in the upper panel. The panel below corresponds to the calibration window highlighted by the green oval.

At the first point of the conductivity range (5.82 S/m), several tests were performed to fix the sensor orientation in the tank and determine the conductivity cell constant. Finally, the sensor was placed in a horizontal position that proved to be the most suitable in order to have a free flow of the water to

the sensing elements (Fig. 18). A constant equal to K = 2.9 was given to CTD through the terminal software and the corresponding commands.

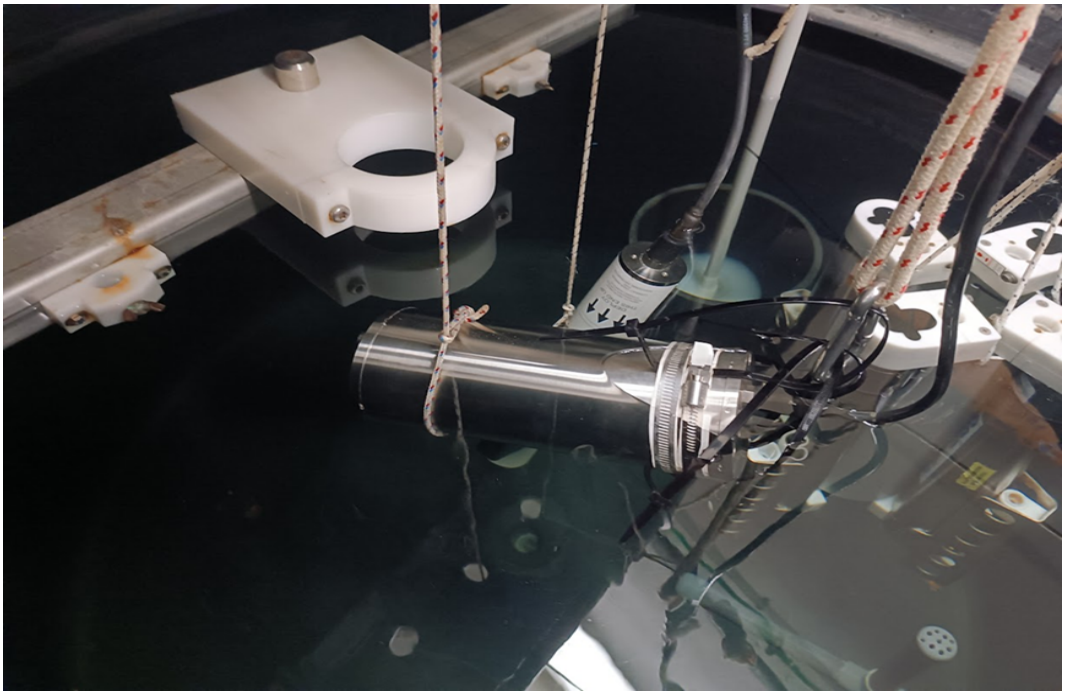

Figure 18: The NAUTILOS CTD placed horizontally inside the tank during the conductivity calibration experiment.

3.4. Results

Temperature

After the analysis of the averaged data in each calibration "window" and the estimated mean values it was possible to proceed to a linear fit of the form:

$$T_{ref} = a*T_{inst} + b$$

where T_{ref} is the value of the SBE-35 reference thermometer, T_{inst} is the value of the NAUTILOS CTD, a= 0.9915 and b = -0.1887 (Fig. 19).

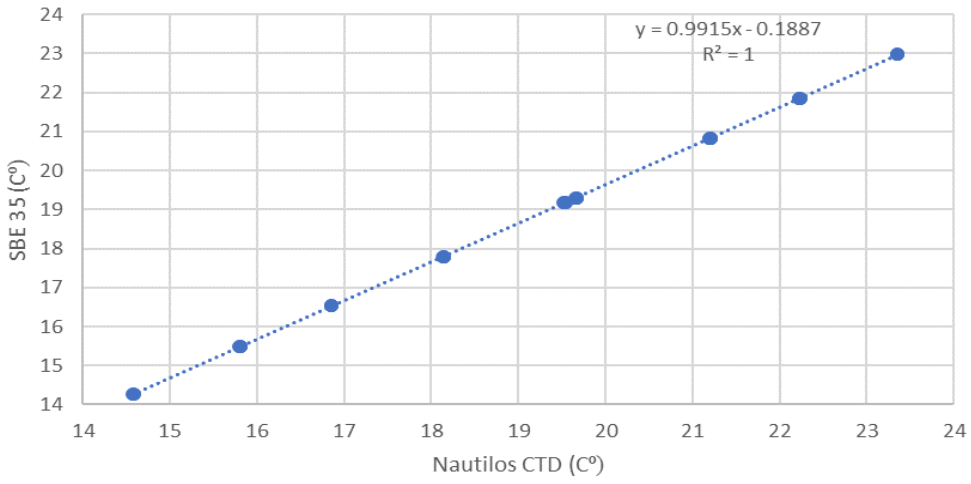

Figure 19: Calibration linear fit for CTD temperature sensor.

The temperature residuals before and after the calibration experiment and the analysis of the data are presented in Fig. 20. The pre-calibration residual between reference T (SBE35) and LMSE RTD is due to inaccurately specified R0 (resistance RTD at zero °C). Sensor temperature (T) is proportional to measured resistance (R) by relation

$$R=R0*(1+TCR*dT).$$

Based on the experimental data analysis a temperature correction coefficient was given to the sensor using the terminal command.

100 setlmsertd 2911 4450

LMSE RTD R0 is set to: 2911.000000 ohm

LMSE RTD TCR is set to: 4450.000000 ppm/'C

The post-calibration results refer to the residuals of the temperature sensors after the adjustment R0 of RTD. (ref: Deliverable 4.5 Report on development and laboratory tests of Deep ocean CTD sensor)

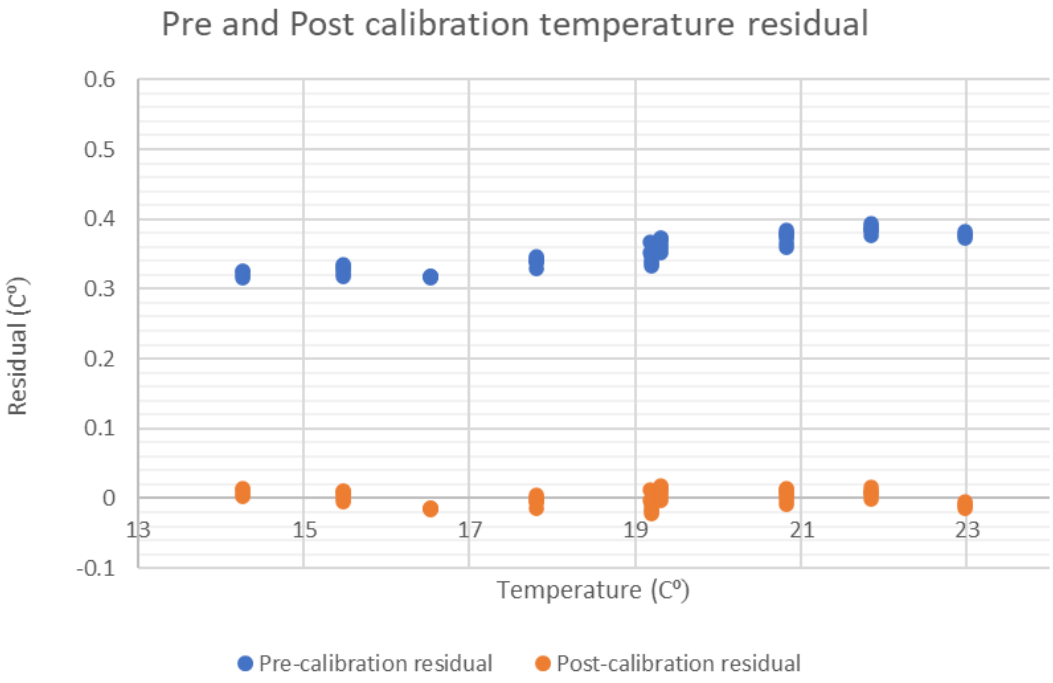

Figure 20: The temperature residuals before and after the calibration of the sensor.

Conductivity

The conductivity sensor is strongly dependent on temperature and compensation for this effect is required to achieve an accurate measurement. Conductivity in the NAUTILOS CTD is temperature compensated at 25 °C as:

$$C\_(comp(25°C))=C\_raw/(1+(TCC*10\^(-2)\ (T-25))\ )$$

By default TCC was set to 2.0. Experiments performed by the sensor developers (Fig. 21) reports that a 3.5 °C variation temperature of the analyte results in 3.68 mS/cm variation of conductivity, if the conductivity compensation in the CTD electronic circuit has been turned off. When compensation is active, conductivity readouts are limited only by electronic noise and time drift of measured

conductivity (0.07 mS/cm/day), indicating that the conditions at the electrodes are changing with time.

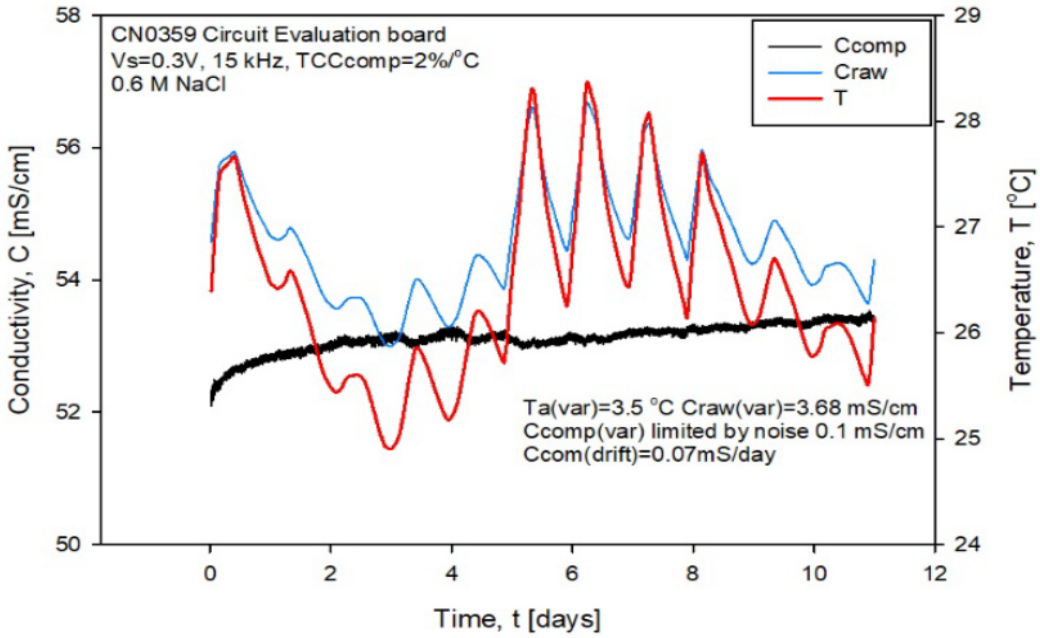

Figure 21: Uncompensated long term measurement of conductivity (blue) at variable room temperature environment (red) and efficient temperature compensation of conductivity by experimentally determined TCC=2% /°C (black).

The conductivity cell constant was determined in the beginning of the experiment where the sea water tank inside the tank had the higher conductivity value of 5.82 S/m. The cell constant of K=2.9 was used in the whole range of conductivity during the experiment. The residual of the conductivity measurement during each step is presented in Fig. 22. The data corresponds to mean values of the residual during each calibration "window". As expected, the residual is higher to lower conductivity values.

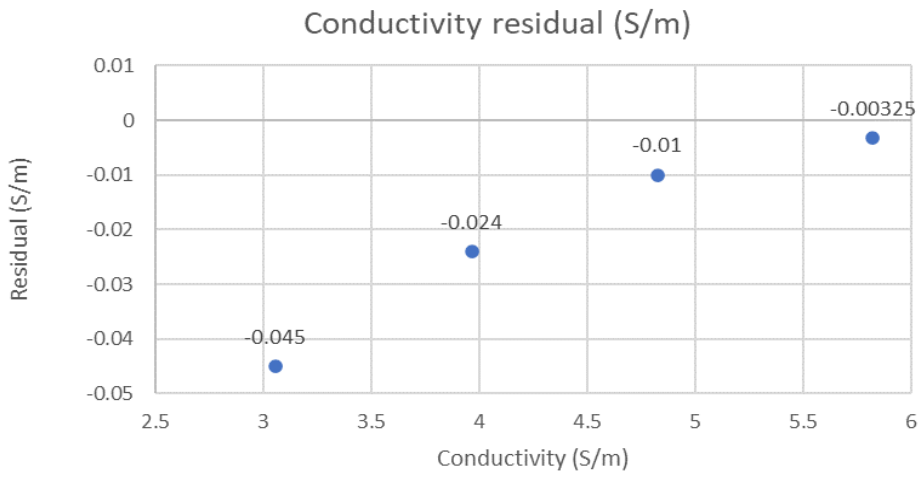

Figure 22: The conductivity residuals before the data process.

Using the same technique as the temperature sensor a linear fit of the form:

Tref = a*Tinst + b

where Tref is the value of the SBE 37 reference conductivity sensor, Tinst is the value of the NAUTILOS CTD, a= 0.982715 and b = 0.0096 can be applied in the data (Fig. 23).

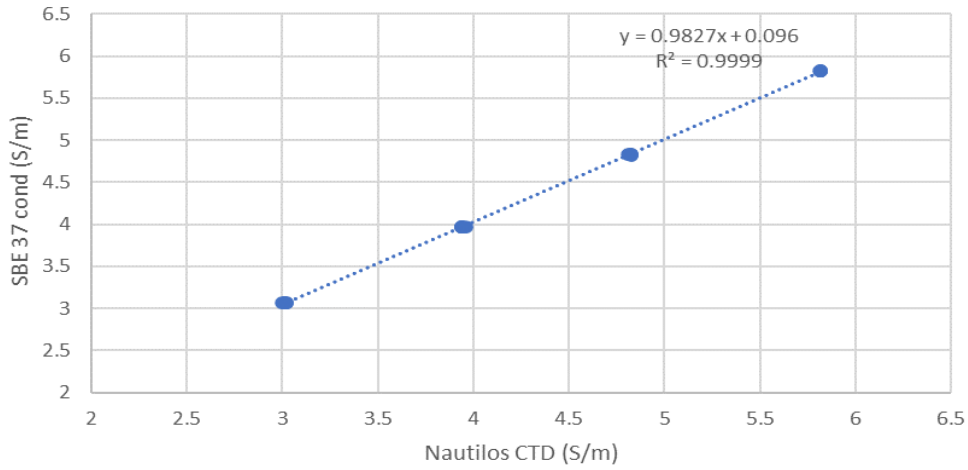

Figure 23: Calibration linear fit for CTD conductivity sensor.

The pre and post calibration conductivity residuals of the CTD using the cell constant of K=2.9 and TCC=2 are presented below in Fig. 24.

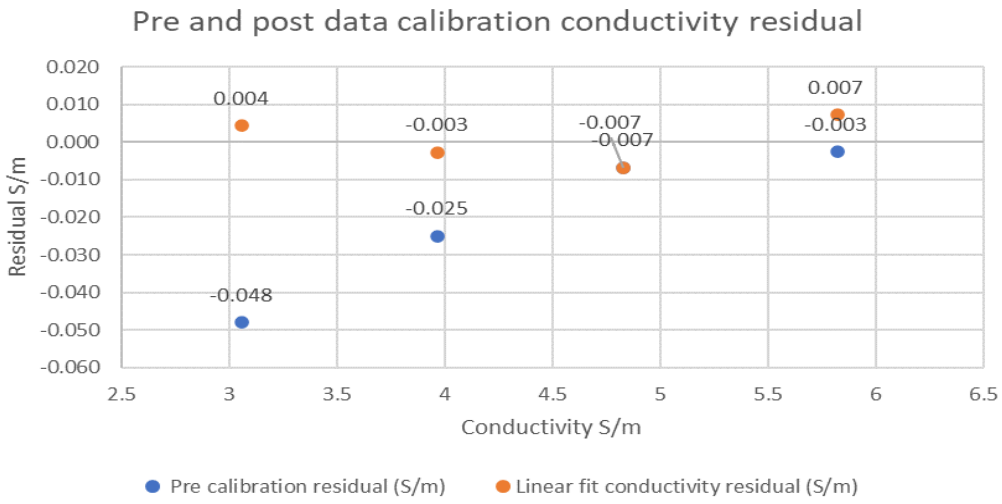

Figure 24: The conductivity residuals before and after the calibration of the sensor.

4. SUBMERSIBLE NANO- AND MICROPLASTICS SAMPLER (SUNAMIPS)

The submersible nano- and microplastic sampler represents a solution for long term deployment and sampling at greater water depth down to 600 m. The first prototype system being used for validation consists of four sample lines, each with 3 different filter meshes, ranging from 300 µm to 30 µm, for

sample pre-sorting. During sampling the system measures the volume flow rate for calculation of particle concentration. After system recovery the samples need to be analysed in order to receive information about number of particles, particle size and material.

Figure 25:The SuNaMiPS with external batteries attached - ready for deployment.

4.1. Objectives

Repeatability and functionality

The goal is to validate the overall functionality of the sampler with a special view on the repeatability of the sampling process.

4.2. Calibration and validation references

To validate the recovery rate, spherical polystyrene (PS) reference particles were used. For the flow and volume calibration a magnetic inductive reference flow sensor was used, ranging from 160 ml/min to 3.2 l/min with an accuracy of 2% full scale.

4.3. Description of the tests

For the validation and calibration of the particle sampler various tests have been performed by SubCtech to assess the sampling and long-term performance of the unit. Some of the tests have been performed in collaboration with NIVA at the NIVA research station in Solbergstrand during a joint workshop with different partners of the NAUTILOS project.

Particle sampling

For the analysis of the samples taken during deployment, one factor is the number of particles found in the sample. Since the particles pass a pump, a volume flow sensor, several centimetres of tubing and the multi valve before they are collected on the filter, a test was performed to evaluate the recovery rate of the sampler.

The test was performed with 10 spherical particles with a diameter of 500 µm. A water container with a known volume of DI water mass was filled with the particles before the water was pumped through the sampler into one of the four filters. To reduce cross contamination the filters were cleaned in an ultrasonic bath with Milli-Q before sampling. After the sampling, the filters were removed from the sampler and sealed with aluminium foil to prevent cross contamination and loss of particles during transport to the lab for further analysis.

In addition to this sample, three more samples were taken with smaller particles and at a known mass. These samples were stored for later analysis as these small particles could not be counted or analysed with the available lab equipment.

Table 10: Reference microplastic particles used for testing.

Sample number	Size	Quantity	Material
Sample 2	150-280 µm	1 mg	PVC
Sample 3	125-150 µm	0.9 mg	PE
Sample 4	100-150 µm	1.3 mg	PS

Volume correction

For the analysis of particle numbers per water volume, the sampler is equipped with a volume flow sensor. During the selection of the flow sensor, an important factor was pressure resistance so that the system can be used at water depths up to 600 m. This led to the selection of a flow sensor that needs additional calibration in combination with the sea water pump used in the system due to low flow rates.

For the calibration the sampler was submerged in a water tank and equipped with an additional flow sensor suitable for the dedicated flow rates in series to the sampler's own flow sensor (Fig. 26). Some samples were taken with a known water volume others were taken over a known time with much larger water mass. To also receive information on the error difference depending on the actual flow rate, the water was equipped with particles that were collected in the filters. This led to partial clogging of the filters resulting in a reduction of the flow rate. In total 14 samples were taken to receive information on the sensor error and repeatability and to apply a correction to the measured water volume.

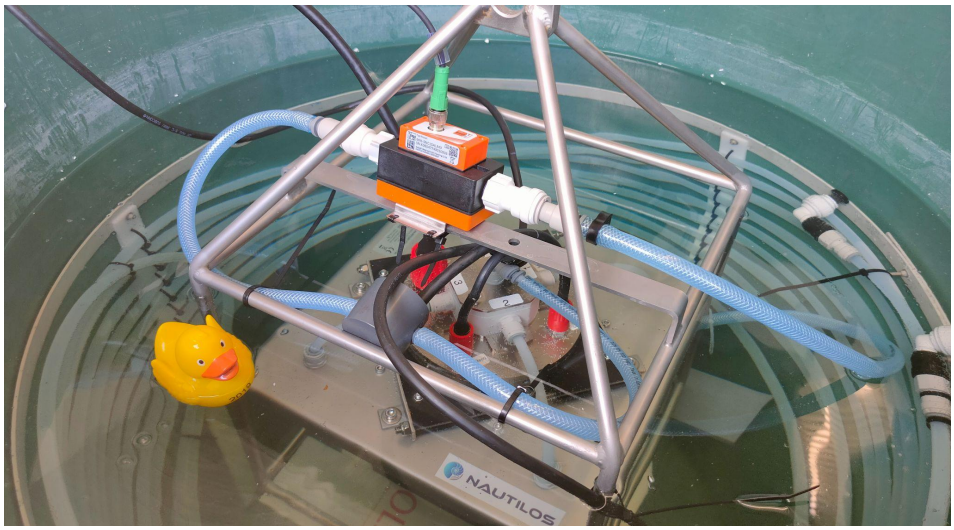

Figure 26: Sampler under testing conditions.

Performance tests

To test the overall sampler performance, the sampler was submerged in a saltwater tank. The system was programmed to perform samples over a period of a month. The purpose of the test was the identification and elimination of bugs and errors that could occur during long term deployment as other system tests were only performed over short periods.

4.4. Results

The overall outcome of the validation experiments of the SuNaMiPS is a good functionality. A summary of the results follows. After the samples were taken for the validation of particle recovery rate, they were shipped to NIVA for analysis. The first sample with PS 500 µm particles showed a recovery rate of 100% (10 of 10 particles were recovered from a 50 L seawater sample). While all three size fraction samples were collected and prepared for the analysis, only the 500 µm particle recovery rate was analysed and the remaining size fractions were stored so the recovery rate can be determined as soon as the needed analytical equipment is available.

During the long-time performance testing an issue was found resulting in incomplete log files. This could be solved and eliminated with a software update.

During the tests for the flow calibration, a significant difference in measured volume flow rate and therefore a significant difference in overall sampled water volume was identified (Figs. 27 and 28).

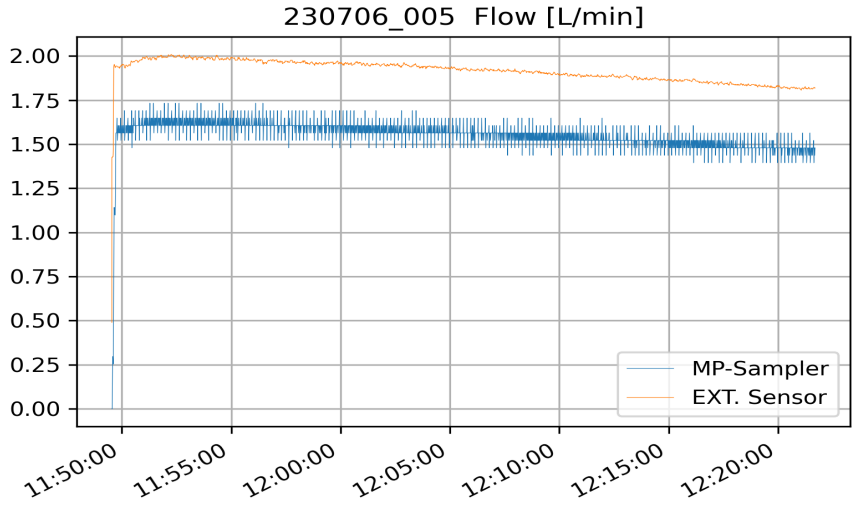

Figure 27: Difference of measured flow rate.

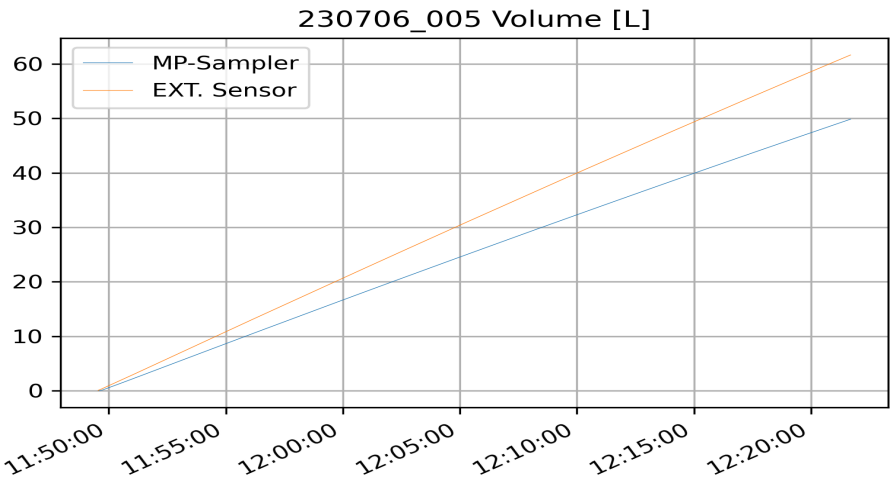

Figure 28: Difference in calculated volume.

The differences in calculated volume ranged from 17.93% to 20.37% with a mean of 18.86% with a standard deviation of 0.87%. The value is constant throughout the range of expected flow rates and over different amounts of sampled water volume. With this, a correction of the measured water volume can be performed. This needs to be done in the post processing but will be implemented in the samplers software after integration and field tests.

Table 11: Results of the water flow measurements.

	Water volume sampler sensor [L]	water volume external sensor [L]	deviation [%]
1	50.06	62.36	19.72
2	50.13	61.78	18.86
3	50.03	61.66	18.86
4	116.78	146.33	20.19
5	279.27	343.58	18.72
6	391.75	491.94	20.73
7	616.08	773.26	20.33
8	732.57	894.41	18.09
9	742.98.	905.3	17.39
10	746.17	911.73	18.16
11	1485.73	1816.46	18.21
12	1492.95	1826.85	18.28
13	1479.83	1808.74	18.18
14	1466.66	1791.75	18.14

5. LOW COST MICROPLASTIC SENSOR (LAMPO)

LAMPO is the acronym for the microplastic sensor being developed and it stands for Low-cost Aquatic MicroPlastic Observation system (Fig. 29). The system consists of a pre-filtration unit with a large-volume pump and mesh filter of 1 mm size, a filtration unit with a mesh size of 300 µm. It also contains a backflush mechanism to transfer the particles to the staining chamber, where the microplastics are stained with Nile red and a second backflush mechanism to transfer the stained microplastic particles to the detector consisting of multiple fluorescence detectors. LAMPO will also contain readout electronics and an integrated computer for device control and data analysis and communication.

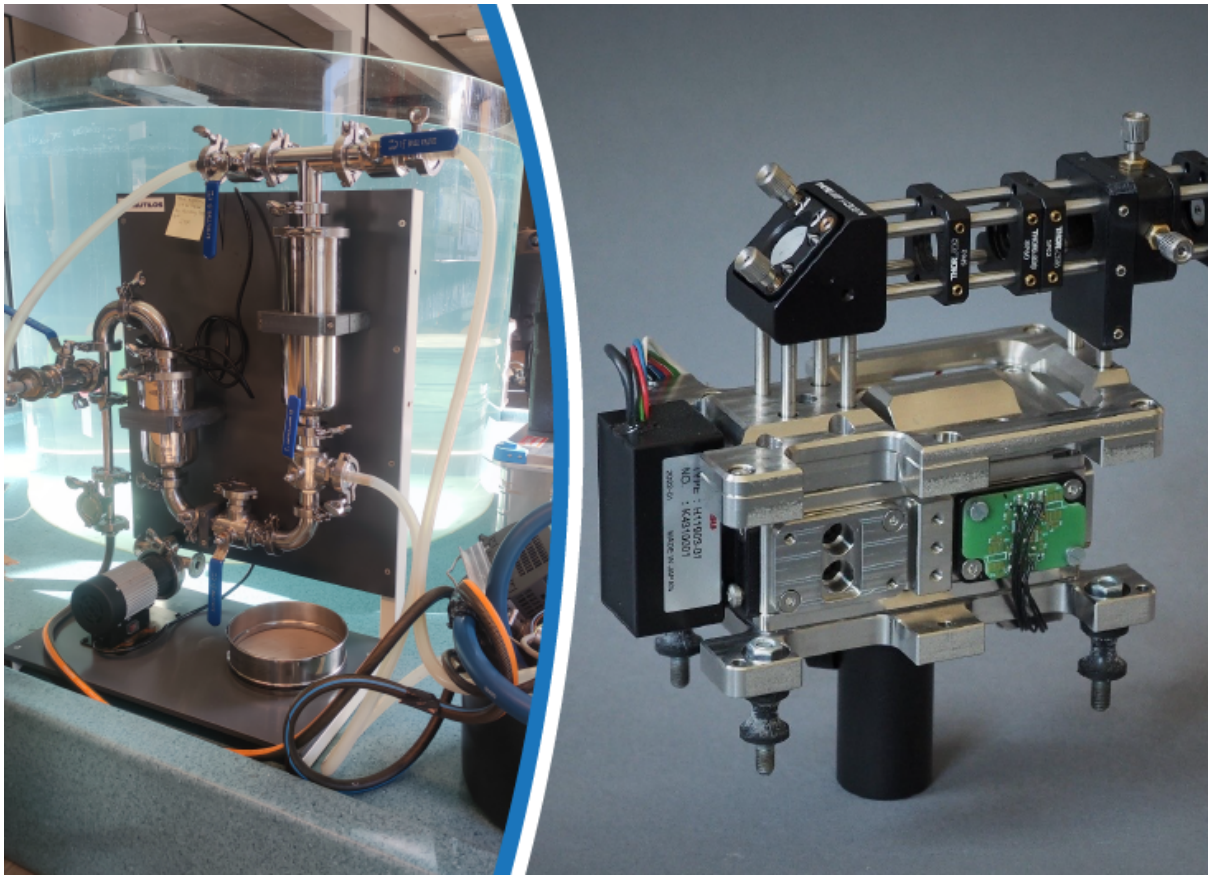

Figure 29: Low cost microplastic sensor.

5.1. Objectives

Accuracy

The aim for the microplastic sensor is to achieve an 80% accuracy and repeatability while measuring microplastics particles in the range between 50 to 300 µm. Achieving a maximum relative standard deviation of 20%. Tests for the calculation of repeatability, accuracy and repeatability, among others, have not been calculated yet since both units have not been connected.

5.2. Calibration and validation references

Two types of spherical microplastic reference materials, transparent PS 500 µm and green PE 710-810 µm were used for testing the different units of the microplastic sampler and to estimate the recovery rate of the system. For testing the fluorescence detector three polymer types, PE (125-150 µm), PS (150-250 µm) and PVC (150-250 µm), were stained with Nile red and particles were transferred and mixed with MilliQ water in beakers (one per polymer type). The solutions were further injected in the fluorescence detector with a syringe to see the difference in signals for the different polymer types.

5.3. Description of the tests

NIVA has conducted numerous tests on the microplastic sampler, evaluating its various components. Recovery tests were carried out by introducing diverse microplastic particles to assess the individual and combined performance of the pre-filtration and filtration units.

Additionally, CSEM's fluorescence detector has undergone testing by both CSEM and NIVA, without integration with the microplastic sampler. The microplastic detector is used for measuring particles within the size range from 50 to 300 µm. Among the most frequently targeted plastics are PE, PP, PET, PS, PA, and PVC, as these polymers are commonly encountered in the marine environment. A test exercise was conducted at Solbergstrand in May 2023, where the different partners worked together

on the microplastic sampler and fluorescence detector. The purpose of sub-task 6.2.5 is to test the combined system of the microplastic sampler and fluorescence detector.

Microplastic sampler working principle and performance

The performance of the pre-filtration and the filtration units was evaluated at NIVA over several months in 2023, and also at the NAUTILOS WP5/WP6 workshop in Solbergstrand in May 2023, by adding microplastics particles into the system with recirculating water from the pre-filtration to the filtration unit. Thereafter, backflush was conducted to transfer particles out from the filtration unit through a hose to exit the system. For future tests, where the "Exit from backflush" hose is located (Fig. 30), the dying unit will be attached at the hose exit point. At this stage, the system has been satisfactorily tested with transparent polystyrene particles with a size of 500 µm and green polyethylene particles ranging from 710 to 810 µm in size. These particles were deliberately chosen as their larger sizes allowed for monitoring their passage through different parts of the sampler, ensuring proper performance of the microplastic sampler.

The process of extracting particles from the filtration unit posed few challenges. This was primarily because, during the backflush, the filtration unit was already filled with water. As a result, the water's force during the backflush was insufficient to expel the particles from the unit effectively. To overcome this issue, it was decided to run the system in normal mode, then proceed to empty and refill it with water from the backflush. In this way all the introduced particles were successfully removed, resulting in a 100% recovery rate in several subsequent tests performed. However, not in all the tests the particles managed to exit the hose therefore the system needs to be adjusted. Figure 30 illustrates one of the two operational run modes for the microplastic sampler, the normal mode. The backflush mode is another operation run mode.

Figure 30: Microplastic sampler normal run mode.

Fluorescence detector working principle and performance

The microplastic detector measures particles directly in the flow (inline measurement). Plastic particles from the staining chamber are backflushed into a glass capillary, where they are illuminated by a strong focused blue laser beam. The fluorescence is then collected with a lens and sent through

a fluorescence filter that transmits only green/red fluorescence light, while rejecting nearly all the scattered blue laser light (Fig. 31).

The microplastic detector performance was evaluated in WP4 and has shown that microplastic in the range of 30-300 µm can be measured as intended. Sample datasets, also included in the deliverable D4.4, are shown in Fig. 32. From these tests we saw the need to optimise the microplastic detector to signal emitted by microplastic in situ (parameters: detector channel gain, peak detector width and noise threshold). Unfortunately, unforeseen problems with the microplastic transfer from sampler to detector have prevented us from tackling this problem. Nevertheless, the measurement process is established and working, including data analysis (see below) and export to open-source FCS file format, with can be viewed in free FCS viewers (e.g. https://floreada.io/).

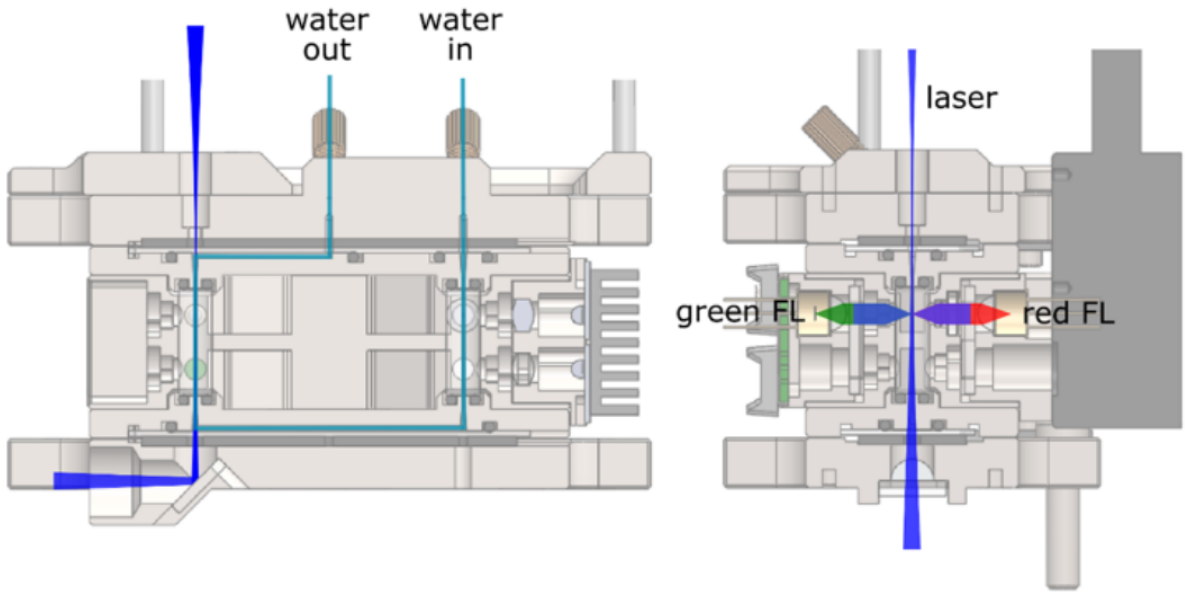

Figure 31: Cross section of the microplastic detector with the fluidic pathway (left) and the green and red fluorescence detection channels on the photodiodes.

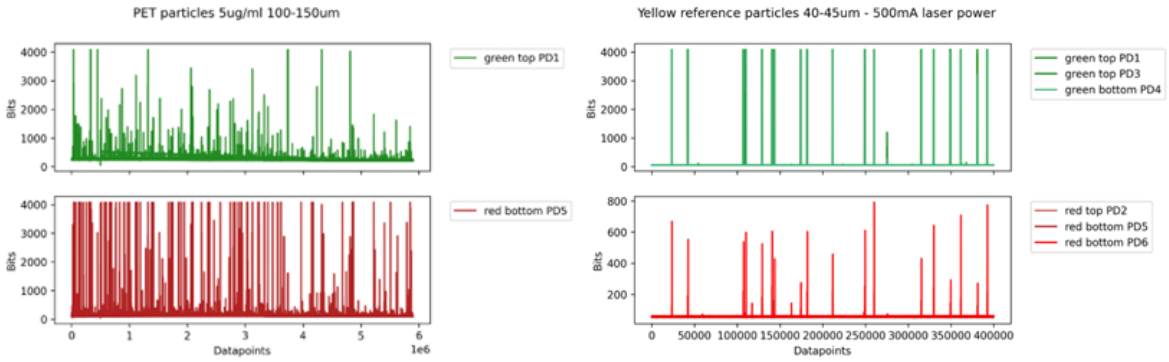

Figure 32: Characterization datasets recorded with the microplastic detector, for Nile red stained PET microplastic 100-150um (top) and yellow reference plastic spheres 40-45 um (bottom).

Microplastic data analysis software

The NAUTILOS Software/User Interface manages the acquisition, storage, and postprocessing of data obtained from the particle detector, with a focus on extracting meaningful information. The postprocessing phase employs filtering algorithms to enhance the raw data and peak identification algorithms for isolating significant peaks corresponding to measured particles. Upon acquisition, the

raw data from the particle detector is stored in a CSV format, organized into segmented files, each containing 50,000 measurement points from the six channels. This segmentation strategy facilitates efficient post-acquisition handling and manipulation of the large data.

Following data acquisition, the raw data undergoes a sequential post-processing workflow involving the application of filtering algorithms to individual segment data files. The software features three distinct filter types—Simple Moving Average (SMA), Gaussian, and low-pass Butterworth. While user-adjustable parameters for these filters are not currently available, they are preconfigured to ensure optimal results. Ongoing efforts are directed towards the optimization of these filter parameters. Once the data is smoothed by the selected filter, a peak-finding algorithm is applied to the segment data file, utilising parameters such as minimum peak separation, expected width range, threshold, minimum amplitude, and prominence. Further optimization of these parameters is underway through testing on real sample data obtained from the system.

To account for time shifts in raw signals from different photodetectors, signal cross-correlation is employed. Photodetectors are currently grouped into clusters according to their physical position, however in the final solution it is planned to be grouped according to spectrum of detection (green vs. red). In the event of peak detection, information is stored in a human-readable JSON format, detailing peak width, height and the corresponding channel of the cluster. If an event is not detected on a specific channel of the cluster, relevant parameters are set to "null" or "0".

The latest software version introduces background signal extraction across all channels, measured at the initial and final second of the recording. Background signal levels per channel are included in the same JSON file. Furthermore, the software facilitates the conversion of extracted peak information into Flow Cytometry Standard files, compatible with various open-source flow cytometry viewers and plotting software.

5.4. Results

During the various tests carried out at NIVA to evaluate the different components of the microplastic sampler, challenges arose when attempting to extract particles from the filtration unit. Despite several tests, a recovery rate above 50% could not be achieved, leading to further investigation. During recent tests, it became apparent that the primary issue was that the filtration unit already contained a lot of water during the backflush process. Consequently, the force of the backflush was insufficient to remove all the particles from the unit. To address this problem, a new approach was adopted. The system was initially run in normal mode, followed by emptying and refilling it with backflush water. This modification led to a few recovery rates of 100 % for PS 500 µm and PE 710-810 µm, where all 10 introduced particles for each polymer type successfully exited the filtration unit during backflush. However not always all the particles exited the system when repeating the same test.

Moving forward, upcoming tests will be conducted attaching the dying unit to the system. Regarding the fluorescence detector, the data needs to undergo processing with specialised software capable of analysing the substantial amount of data generated.

The next stage involves few improvements on the microplastic samplers so that all the particles exit the system when introduced. Further tests with the attachment of the dying unit into the microplastic sampler system shall be conducted. Recovery tests will be conducted adding the same polymer types; PS 500 µm and PE 710-810 µm and recovery rates will be calculated. Thereafter tests with smaller particles., i.e., 50-300 µm, shall be conducted and recovery rates calculated. All of this has to be taken into consideration and improvements must be made before integration of the microplastic sampler and the fluorescence detector. However, one of the main challenges is still to combine macro fluids (sampling volumes > 1000 L) and microfluidics (mL) into the laser-based fluorescence detection system.

The microplastic detector performance was evaluated at NIVA by analysing triplicate samples of various polymer types and size fractions, including PE (125-150 µm), PS (150-250 µm) and PVC (150-250 µm), all stained with Nile red. Microplastic datasets were acquired and processed with the microplastic detector software. The datasets show only background noise and no detected peaks, contrary to datasets acquired earlier (Sec. 5.1.2). The reasons could be that the microplastic was not transferred from the sampler to the detector properly, or that the laser was badly misaligned.
Improvements need to be made in the form of a photodiode that checks the laser alignment, and more immediate feedback to the user that the measured data includes microplastic peak events. With the new data analysis software described in 5.1.3, this last point should be solved now. Further tests are planned to validate performance of the microplastic measurement system.

6. DEEP-OCEAN LOW-LEVEL RADIOACTIVITY SENSOR

The new radioactivity ocean sensor (Fig. 33) for the deep systems is an additional activity with respect to the Grant Agreement but is reported here as additional work performed. The sensor consists of a detection crystal, connected with a photomultiplier tube, preamplifier, amplifier and power supply, together with a multichannel analyser for data acquisition and storage. The electronic modules are especially constructed to fit inside the detector housing and the power consumption is relevant low (~1 W) in continuous mode of operation. The energy calibration is checked using the photopeak of 40K which is always present at the oceans as a natural constituent of the seawater. A watertight cylindrical enclosure houses the above-mentioned modules together with the digital units. The enclosure offers continuous functionality up to 5000 m water depth and continuous operation since it is tested in a special laboratory for pressure tests. The selection criterion for the appropriate enclosure material is based on minimising the gamma-ray absorption and maximising the pressure tolerance. The ocean gamma-ray spectrometer was connected with a special battery to power the detection system. The enclosure of the spectrometer and the subsea battery box is also tested for high pressures using a special pressure tank. During the last face of pressure tests, the enclosure provided a tolerance up to 500 Atm. The radioactivity sensor is calibrated (in terms of energy, energy resolution and full energy photopeak efficiency) from energy threshold to 2800 keV and tested for its stability to temperature variations. The efficiency calibration and quantification method (in Bq/m3) evaluation were also performed in the calibration tank.

Figure 33: Deep-ocean low-level radioactivity sensor.

6.1. Objectives

The ocean sensor is calibrated (energy, energy resolution) from energy threshold to 2800 keV and tested for its stability to temperature variations. The sensor was required to be calibrated first in the laboratory. This calibration was performed with seven specific point sources of γ-radiation, which

were placed in fixed geometry. Measurements of the detector efficiency and absolute calibration (in Bq/m^3) have also been performed in the water environment (controlled environment). For this purpose, a calibration tank of 5.5 m^3 volume filled with water has been used. The ocean radioactivity sensor was mounted in the middle of the tank in order to be surrounded by one metre of water, which is enough to simulate the high attenuation of the γ-rays (for Eγ<1100 keV). At the bottom of the tank, an electric pump was used to circulate the water, to mix the appropriate radionuclides (^{137}Cs and ^{40}K) with the water and to get homogenous conditions.

6.2. Calibration and validation references

The equipment that was used as a reference equipment is the GeoMAREA system. Secondary reference system is the KATERINA system. KATERINA is a low resolution marine radioactivity system for intermediate water masses (maximum depth of deployment 400 m).

6.3. Description of the tests

The new radioactivity ocean sensor for the deep systems consists of a detection crystal, connected with a photomultiplier tube, preamplifier, amplifier and power supply, together with a multichannel analyser for data acquisition and storage. The electronic modules are especially constructed to fit inside the detector housing and the power consumption is relatively low (~1 W) in continuous mode of operation. The energy calibration is checked using the photopeak of ^{40}K which is always present at the oceans as a natural constituent of the seawater. A watertight cylindrical enclosure houses the above-mentioned modules together with the digital units. The enclosure offers continuous functionality up to 5000 m water depth and continuous operation since it is tested in a special laboratory for pressure tests (Fig. 34). The selection criterion for the appropriate enclosure material is based on minimising the gamma-ray absorption and maximising the pressure tolerance. The ocean gamma-ray spectrometer was connected with a special battery to power the detection system. The enclosure of the spectrometer and the subsea battery box is also tested for high pressures using a special pressure tank. During the last phase of pressure tests, the enclosure provided a tolerance up to 500 Atm. The radioactivity sensor is calibrated (in terms of energy, energy resolution and full energy photopeak efficiency) from energy threshold to 2800 keV and tested for its stability to temperature variations. The efficiency calibration and quantification method (in Bq/m^3) evaluation were also performed in the calibration tank.

Figure 34: The pressure tests were performed in the "Demokritos" laboratory.

This calibration of the ocean radioactivity sensors was performed first in the MERL lab of HCMR in the air by using specific point sources of γ-radiation (e.g. ^{137}Cs, ^{60}Co), which were placed in fixed geometry.

6.4. Results

In the next graphs, the calibrated spectra of the aforementioned point sources are depicted. In Fig. 35 we present the data in log scale in order to energy the sum peak of ^{60}Co at around 2500 keV. Fig. 36 shows data on a linear scale.

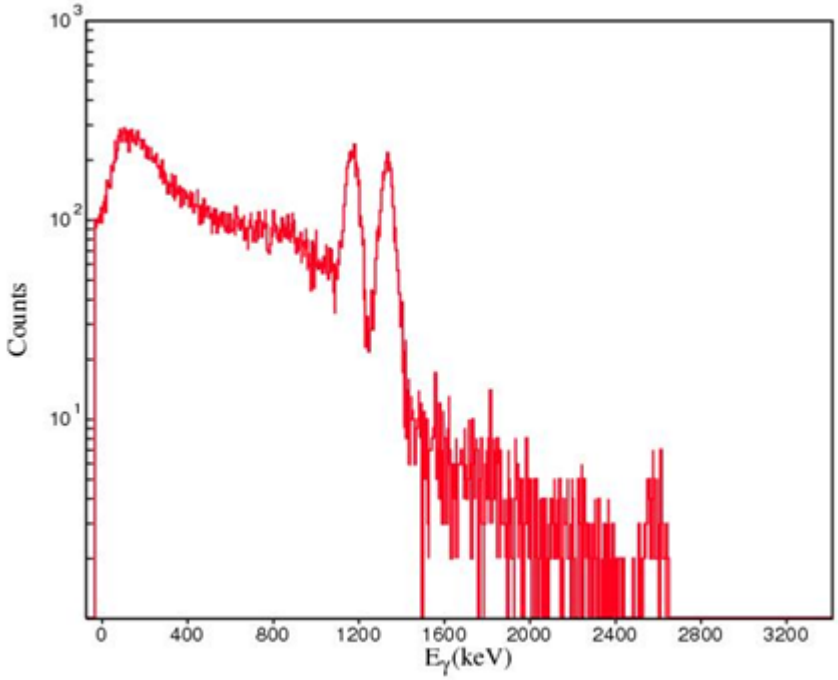

Figure 35: The energy calibrated spectrum using the Co-60 point standard source on log scale.

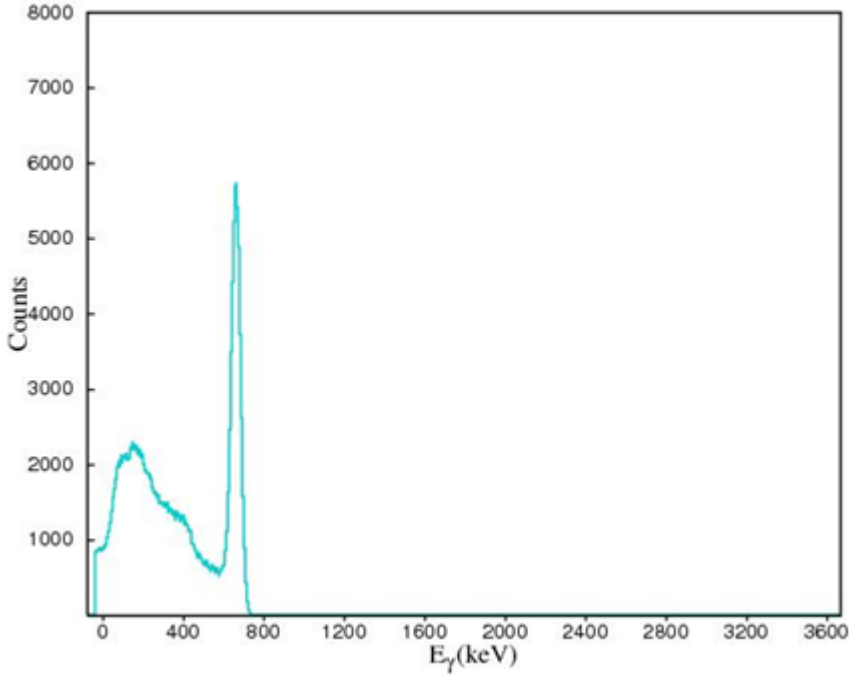

Figure 36: The energy calibrated spectrum using the Co-60 point standard source on linear scale.

Calibration in the water tank

The calibration of the system was performed in a calibration tank of 5.5 m^3 volume filled with fresh water (collaboration with National Technical University of Athens). The underwater detector was mounted in the middle of the tank in order to be surrounded by one metre of water, which is enough to simulate the high attenuation of the γ-rays (for Eγ<1100 keV). At the bottom of the tank, an electric pump was used to circulate the water, to mix the appropriate radionuclides with the water and to get homogenous conditions. The γ-rays used to perform the calibration of the system were 661.6 keV of ^{137}Cs and the 1460.6 keV of ^{40}K. More specifically, 199 g natural KCl was diluted in the tank. Furthermore, liquid Cs-137 with known activity was mixed in the water together with 65% HNO_3 0.005N. The acquired spectra diluting the two reference sources in the tank are shown in Fig. 37 (K-40 and Cs-137) together with the radon progenies (Pb-214, Bi-214) as constituents of groundwater. The analysis of the spectra has been performed with the "SPECTRW" software package. The energy calibration and the FWHM are not changed when the system operates in the aquatic and air environments.

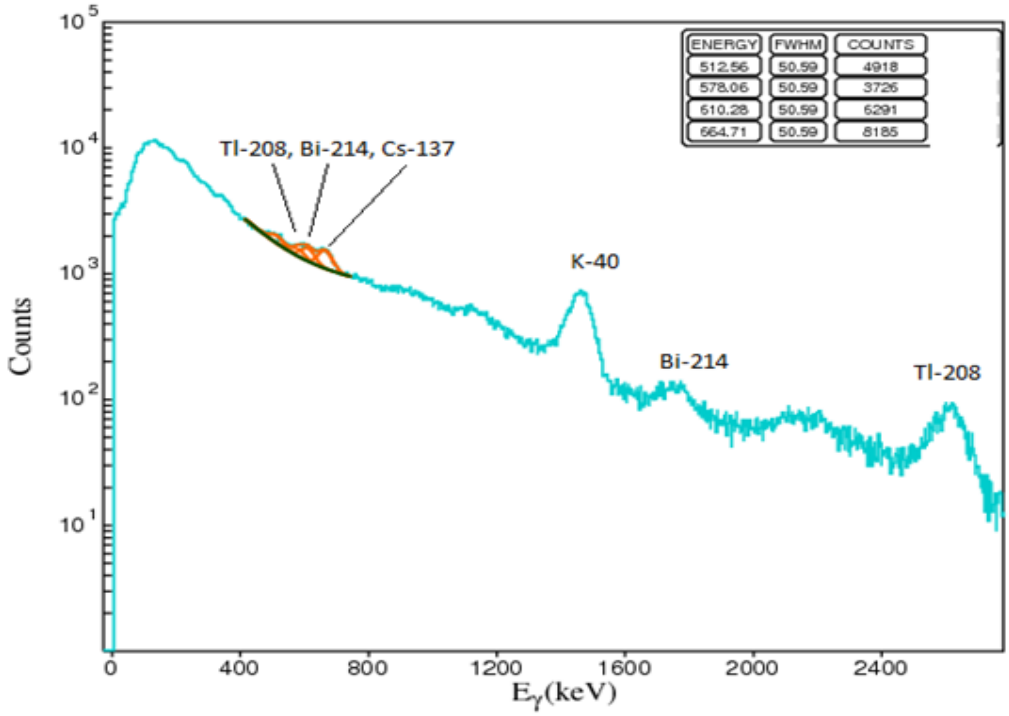

Figure 37: The energy spectrum was acquired in the calibration tank. The detected radionuclides are indicated in the graph. Natural Radioactivity (thoron and radon progenies, K-40) and Artificial Radioactivity (Cs-137) is depicted (Cs-137 at 662 keV, Bi-214 at 609 and 1761 keV, Tl-208 at 583 and 2614 keV, K-40 at 1461 keV).

The operation of the system exhibits the following advantages:

- The energy calibration of the system in the aquatic environment is similar compared with the calibration factors measured in the laboratory with point sources.
- The marine efficiency (in m^3) offers the activity concentration in Bq/m^3 for each detected gamma emitter.
- The design of the electronic components exhibits low dead time values (<0.5%). The system is tested for deployments up to 4500m and can perform measurements autonomously without computer connection.
- The energy window for detecting gamma ray emitters is adjustable.
- The system can be stabilised in terms of voltage output using the two photopeaks (1461 keV of $^{40}K40$ and 2615 keV of ^{208}Tl).

IV. SUMMARY

This deliverable reports on the calibration and validation activities from Task 6.2 which includes physical, chemical, and microplastics instruments developed in WP4 of NAUTILOS. Various calibration and validation activities took place under various testing scenarios including test tanks in the laboratory and controlled tests in nearshore environments, and the activities also incorporated various reference instruments, reference materials, and other calibration materials. Key findings, limitations, TRL, and future work are presented for each subtask below.

Carbonate system sensors: Preliminary tests and calibration checks were performed in the laboratory, and the sensors, and the sensors were considered ready for demonstration in WP7. Both the pH and CO2 sensors were able to achieve "weather" uncertainty objectives of ~±0.02 and ±2.5%, respectively. Some additional tests will be carried out related to ISFET sensor conditioning. Continued work related to long-term drift and calibration reliability will also be carried out until the beginning of WP7 demonstrations. We consider the pH and CO_2 sensors presently at a technological readiness level of 5 and reach level nine 9 by the end of the project.

Silicate Sensor: The silicate electrochemical sensor showed an accuracy better than 2% measuring CRM solutions after being calibrated with silicate standards diluted in artificial seawater within concentration range observed in open ocean. The results obtained and reported in these deliverable highlighted targeted performances of the sensor compatible with its use on profiling floats. The instrument is currently at TRL 6.

Deep ocean CTD: The NAUTILOS CTD instrument for deep ocean measurements has undergone testing and calibration in a laboratory environment at PCL within specified temperature and conductivity ranges, which are representative of the East Mediterranean Sea environment. The calibration results achieved meet the sensor specifications previously established during the instrument's development phase by experiments conducted at UL-FE. Additionally, new calibration coefficients have been generated to account for realistic environmental parameter ranges. The TRL of the deep ocean CTD instrument is currently at TRL 6. This suggests that the instrument has reached a stage where it has been validated in a relevant environment and is ready for further field testing and demonstration.

SuNaMiPS: The calibration/validation led to a correction of the flow and volume data to achieve best results for particle concentration. The recovery rate could only be analysed with 500 µm particles in which recovery was 100%. Further samples need analysis at a later stage of the project as the analytical equipment was not available at this point. The samples were preserved and stored. The sampler is currently at a TRL 6.

Low cost Microplastic sensor (LAMPO): Several tests have been conducted in the laboratory on the microplastic sampler to evaluate its different components. These tests have indicated the need for adjustments in certain parts to enhance the system's overall performance. Additionally, experiments have been performed on the laser detector using diverse polymer types and size fractions, but the data from these experiments are yet to undergo analysis. Nonetheless, the integration of both systems is still pending due to limitations associated with the necessity to reduce the high flow rate, which is crucial for efficiently flushing particles from the filtration unit into the staining chamber before their transfer to the laser detector. As each component can be individually operated, microplastic sampler component is currently TRL 6, the laser detector component is TRL 4, and the complete sensor (sampler + detector) has not yet been achieved and is therefore currently TRL 3.

Deep ocean Radioactivity sensor: A new detection radioactivity system for the deep ocean was developed and applied in the laboratory for calibration for determining the radioactivity levels in aquatic systems. This work was performed in addition to what was defined in the Grant Agreement for D6.2. The enclosure of the system was tested for pressure tolerance. The system reaches at this

stage the TRL 6 since its components and the whole technology are validated in a laboratory environment.

V. APPENDIX 1: REFERENCES AND RELATED DOCUMENTS

ID	Reference or Related Document	Source or Link/Location
	Bresnahan, P.J., Martz, T.R., Takeshita, Y., Johnson, K.S., LaShomb, M., 2014. Best practices for autonomous measurement of seawater pH with the Honeywell Durafet. Methods Oceanogr. 9, 44–60.	https://doi.org/10.1016/j.mio.2014.08.003
	Newton, J.A., Feely, R.A., Jewett, E.B., Williamson, P., Mathis, J., 2015. Global Ocean Acidification Observing Network: Requirements and Governance Plan, Second Edi. ed. GOA-ON.	http://www.goa-on.org/documents/general/GOA-ON_2nd_edition_final.pdf
	Dickson, A.G., Sabine, C.L., Christian, J.R. (Eds.), 2007. Guide to best practices for ocean CO2 measurements. PICES Special Publication 3. North Pacific Marine Science Organisation.	https://www.ncei.noaa.gov/access/ocean-carbon-acidification-data-system/oceans/Handbook_2007.html
	Grasshoff, K., Kremling, K., Ehrhardt, M., 1999. Methods of Seawater Analysis, 3rd ed, Methods of Seawater Analysis: Third, Completely Revised and Extended Edition. Wiley.	https://doi.org/10.1002/9783527613984
	Lewis, E., Wallace, D.W.R., 1998. Program developed for CO2 system calculations. Carbon Dioxide Inf. Anal. Center, Oak Ridge Natl. Lab.	https://doi.org/10.15485/1464255
	van Heuven, S., Pierrot, D., Rae, J.W.B., Lewis, E., Wallace, D.W.R., 2011. MATLAB Program Developed for CO2 System Calculations. ORNL/CDIAC-105, Carbon Dioxide Inf. Anal. Center, Oak Ridge Natl. Lab. US Dep. Energy.	https://doi.org/10.3334/CDIAC/otg.CO2SYS_MATLAB_v1.1
	Mehrbach, C., Culberson, C.H., Hawley, J.E., Pytkowicz, R.M., 1973. Measurement of the	https://doi.org/10.4319/lo.1973.18.6.0897

	apparent dissociation constants of carbonic acid in seawater at atmospheric pressure. Limnol. Oceanogr. 18, 897–907.	
	Dickson, A.G., Millero, F.J., 1987. A comparison of the equilibrium constants for the dissociation of carbonic acid in seawater media. Deep Sea Res. Part A. Oceanogr. Res. Pap. 34, 1733–1743.	https://doi.org/10.1016/0198-0149(87)90021-5
	Dickson, A.G., 1990. Standard potential of the reaction: AgCl(s)+HCl(aq), and and the standard acidity constant of the ion HSO4− in synthetic sea water from 273.15 to 318.15 K. J. Chem. Thermodyn. 22, 113–127.	https://doi.org/10.1016/0021-9614(90)90074-Z
	Uppström, L.R., 1974. The boron/chlorinity ratio of deep-sea water from the Pacific Ocean. Deep Sea Res. Oceanogr. Abstr. 21, 161–162.	https://doi.org/10.1016/0011-7471(74)90074-6
	Orr, J.C., Epitalon, J.-M., Dickson, A.G., Gattuso, J.-P., 2018. Routine uncertainty propagation for the marine carbon dioxide system. Mar. Chem. 207, 84–107.	https://doi.org/10.1016/j.marchem.2018.10.006
	Gattuso, J.-P., Epitalon, J.-M., Lavigne, H., Orr, J., 2021. seacarb: seawater carbonate chemistry. R package.	https://cran.r-project.org/web/packages/seacarb/index.html
	Weiss, R.F., 1974. Carbon dioxide in water and seawater: the solubility of a non-ideal gas. Mar. Chem. 2, 203–215.	https://doi.org/10.1016/0304-4203(74)90015-2
	Takahashi, T., Olafsson, J., Goddard, J.G., Chipman, D.W., Sutherland, S.C., 1993. Seasonal variation of CO_2 and nutrients in the high-latitude surface oceans: A comparative study. Global Biogeochem. Cycles 7, 843–878.	https://doi.org/10.1029/93GB02263
	Martz, T., Daly, K., Byrne, R., Stillman, J., Turk, D., 2015. Technology for Ocean Acidification Research: Needs and Availability. Oceanography 25, 40–47.	https://doi.org/10.5670/oceanog.2015.30
	Reggiani, E.R., King, A.L., Norli, M., Jaccard, P., Sørensen, K., Bellerby, R.G.J., 2016.	https://doi.org/10.1016/J.JMARSYS.2016.03.017

	FerryBox-assisted monitoring of mixed layer pH in the Norwegian Coastal Current. J. Mar. Syst. 162, 29–36.	
	Ntoumas, M., Perivoliotis, L., Petihakis, G., Korres, G., Frangoulis, C., Ballas, D., Pagonis, P., Sotiropoulou, M., Pettas, M., Bourma, E. and Christodoulaki, S., et al 2022. The POSEIDON Ocean Observing System: Technological Development and Challenges. J. Mar. Sci. Eng. 2022, 10(12), 1932;	https://doi.org/10.3390/jmse10121932
	Peter M. Saunders, K-H. Mahrt, Robert T. Williams-WHP Operations and Methods Standards and Laboratory Calibration,	WHP Operations and Methods, July 1991, Standards and Laboratory Calibration report
	Sara Pensieri, Roberto Bozzano, M. Elisabetta Schiano, Manolis Ntoumas, Emmanouil Potiris, Constantin Frangoulis, Dimitrios Podaras and George Petihakis. Methods and Best Practice to Intercompare Dissolved Oxygen Sensors and Fluorometers/Turbidimeters for Oceanographic Applications. Sensors 16(5):702 · May 2016. DOI: 10.3390/s16050702	DOI: 10.3390/s16050702
	Ntoumas M., D. Kassis, M. Potiris, D. Ballas, T. Chondronasios, P. Pagonis, T. Tsagaraki, D. Podaras, L. Manousakis, V. Zervakis, P. Drakopoulos, G. Petihakis, and K. Nittis, Activities of the calibration laboratory at HCMR-Crete – progress and challenges, Proceedings of the Sixth International Conference on EuroGOOS, EuroGOOS, H. Dahlin, N.C. Flemming, S.E. Peterson Editors, Publication n. 30, 15-22, (2014),	ISBN 978-91-974828-9-9
	Joint Committee for Guides in Metrology Evaluation of measurement data - Guide to the expression of uncertainty in measurement (GUM) JCGM. 100:2008.	http://www.bipm.org/utils/common/documents/jcgm/JCGM_100_2008_E.pdf